RETINAL CHARACTERIZATION OF THE THY1-GCAMP3 TRANSGENIC MOUSE LINE

by

Stephanie Nicole Blandford

Submitted in partial fulfillment of the requirements
for the degree of Master of Science

at

Dalhousie University
Halifax, Nova Scotia
June 2016

Dedication

To my parents.
For pushing me when I need to be pushed,
inspiring me when I need inspiration,
believing in me when I don't,
and always loving me.
Thank you

Table of Contents

List of Tables

List of Figures

Abstract

The Thy1-GCaMP3 transgenic mouse expresses the genetically encoded Ca^{2+} indicator GCaMP3 in excitatory projection neurons in the central nervous system. This line has the potential to be a valuable research tool for retina research, however very little is known about its performance in the retina. Therefore, the objective of this thesis was to characterize the anatomical and functional properties of GCaMP3 expressed in retinal ganglion cells and to assess whether these properties change in a model of ganglion cell damage, optic nerve transection. Retinas from Thy1-GCaMP3 mice were examined with conventional Ca^{2+} imaging. In a subset of animals, ONT was performed in one eye one, three, five or seven days prior to sacrifice and calcium imaging. Retinas were mounted and transient increases of $[Ca^{2+}]_i$ evoked by superfusion of kainic acid (KA; 10 μM, 50 μM, 100 μM). After Ca^{2+} imaging, retinas were fixed and processed for immunohistochemistry with antibodies against RBPMS (an RGC specific marker) and ChAT (a selective cholinergic amacrine cell marker). In Thy1-GCaMP3 mice, GCaMP3 was widely and uniformly expressed in the ganglion cell layer, and responded to elevated $[Ca^{2+}]_i$ evoked by KA with robust increases in fluorescence intensity. Following ONT, baseline fluorescence reported by GCaMP3 was not altered, and at three, five and seven days post-ONT there was a significant decrease in transient amplitude evoked by all concentrations of KA tested. This suggests that RGCs display a decline in cellular responsiveness prior to cell death. In addition, fewer cells were able to respond to modest concentrations of applied extracellular KA indicating that functional experiments to accompany anatomical data in injury models is critical to developing the most accurate timelines of injury progression. Immunohistochemical analysis revealed that GCaMP3 was expressed in many, but not all $RBPMS^+$ RGCs, and rarely in $ChAT^+$ amacrine cells in both control and ONT retinas suggesting expression is in RGCs and not cholinergic amacrine cells. Furthermore, the proportion of $GCaMP^+$ cells that were also labeled with RBPMS or ChAT did not change following ONT. Therefore, the current work provides evidence that GCaMP3 persistently reports intracellular calcium transients evoked by KA application in RGCs both in the absence and presence of axonal injury, and that GCaMP3 expression is likely restricted to RGCs, and does not change following ONT. The use of the Thy1-GCaMP3 transgenic mouse as a tool for future retina research is promising as it will allow functional assessment of RGCs over time.

List of Abbreviations Used

$[Ca^{2+}]$	Calcium concentration
$[Ca^{2+}]_i$	Intracellular calcium concentration
AAV	Adeno-associated virus
AMP	Adenosine monophosphate
AMPA	α-amino-3-hydroxy-5-methyl-4-isoxazole propionic acid
AP	Action potential
au	Arbitrary unit
BAPTA	1,2-bis-(2-aminophenoxy)ethane-N,N,N',N'-tetraacetic acid
BFP	Blue fluorescent protein
Ca^{2+}	Calcium
cGMP	Cyclic guanosine monophosphate
CFP	Cyan fluorescent protein
ChAT	Choline acetyltransferase
CI	Confidence interval
CNS	Central nervous system
cpGFP	Circularly permuted green fluorescent protein
EGTA	Ethylene glycol-bis(β-aminoethyl ether)-N,N,N',N'-tetraacetic acid
ER	Endoplasmic reticulum
ERG	Electroretinogram
FRET	Fluorescence (Förster) resonance energy transfer
GABA	Gamma-aminobutyric acid
GCL	Ganglion cell layer
GECI	Genetically encoded calcium indicator
GFP	Green fluorescent protein
HBSS	Hanks balanced salt solution
INL	Inner nuclear layer
IOP	Intraocular pressure
IP_3	Inositol triphosphate
K^+	Potassium
KA	Kainic acid
ME	Margin of error
Na^+	Sodium
NCAR	Non-carrier
NFL	Nerve fiber layer
ONL	Outer nuclear layer
ONT	Optic nerve transection
OPL	Outer plexiform layer
PBS	Phosphate buffered saline
PBST	Phosphate buffered saline with triton-X
PDE	Phosphodiesterase
PFA	Paraformaldehyde
PRL	Photoreceptor layer

PTP	Permeability transition pore
RBPMS	RNA-binding protein with multiple splicing
RGC	Reginal ganglion cell
ROI	Region of interest
ROS	Reactive oxygen species
RPE	Retinal pigment epithelium
RT	Room temperature
VGCC	Voltage gated calcium channel
YFP	Yellow fluorescent protein

Acknowledgments

First, to my supervisors. **Dr. Bill Baldridge**, your support, guidance and training over the last three years have truly been invaluable. Thank you for giving me my first shot at research and for all of the opportunities you have provided me with since. Learning from you has truly been a privilege. To **Dr. Spring Farrell**, I wouldn't be here if it weren't for you. You have both played instrumental roles in making me into the scientist I am today, and for that, I will be forever grateful.

To my supervisory committee **Dr. Balwantray Chauhan**, and **Dr. Ying Zhang**, and to my examiner **Dr. Steven Barnes**; thank you all of your time, support, and invaluable advice throughout the course of my degree. From all of you, I have learned and developed a bigger skill set than I ever would have expected that I will carry with me for the rest of my career.

To **Michele Archibald**, thank you for your technical expertise and your moral support. Thank you for the time you spent in the surgery suite for me, your work was instrumental in this project and so appreciated. I will miss sitting next to you, I couldn't have asked for a better desk mate.

To all of my colleagues in the Retina and Optic Nerve Research lab and the Department of Medical Neuroscience, thank you. You have all made the last three years more memorable than I ever could have imagined. **Elizabeth Cairns**, **Corey Smith, Janette Nason, and Sophie Thapa** thank you for everything you've done for me over the years. The list is long. **Lauren Landoni**, you'll always be the one in the room I'll want to be friends with; you and **Kaitlyn Keller** have been the best friends I could have ever hoped for. Thank you both for your moral support, your love, and for just being you.

To my siblings. **Claudia Blandford**, thank you for doing everything a big sister is supposed to. For listening to me whine, picking me up when I'm down, challenging me, questioning me, and arguing with me. You've taught me to think for myself and stand by my convictions. Also, thank you for your artistic talent. I've always been jealous of it. **Paul Blandford**, thank you for helping me move all of my furniture to avoid bedbugs, and for shoveling my car out from 4 feet of snow. Thank you for always being there when I need you. You have no idea how much I appreciate it.

To the countless others who contributed in one way or another to my growth as a person and as a scientist. Thank you.

Chapter 1: Introduction

1.1 The Retina

Vision is one of the five senses that allow us to perceive and navigate our environment. The ability to see begins with the eye. Light enters via the pupil and is focused on the retina by the cornea and lens. The amount of light that enters the eye is controlled by the iris, which alters the diameter of the pupil in response to changing light intensities in the environment. The retina is a thin, multilayered arrangement of neural tissue that lines the back of the eye. This tissue is responsible for sensing light from the environment and converting it into an electrochemical signal that is processed and propagated through various cell types before being transmitted to visual centers in the brain to allow visual perception (Sanes and Zipursky, 2010).

The mammalian retina is a laminated tissue (Figure 1.2). The deepest (most posterior) layer, adjacent to the retinal pigment epithelium (RPE), is the photoreceptor layer (PRL) that contains the light-sensitive outer segments of rod and cone photoreceptors. The outer nuclear layer (ONL) contains the cell bodies of the photoreceptors. The outer plexiform layer (OPL) contains synapses between photoreceptor terminals (rod spherules and cone pedicles) and bipolar cell and horizontal cell dendrites. Cell bodies of bipolar cells, horizontal cells, amacrine cells and displaced RGCs are contained in the inner nuclear layer (INL). Synapses between bipolar cells, amacrine cells and retinal ganglion cells (RGCs) reside in the inner plexiform layer. RGC somas, and displaced amacrine cells form the ganglion cell layer (GCL), and RGC axons form the nerve fiber layer (NFL) before exiting the eye as the optic nerve through

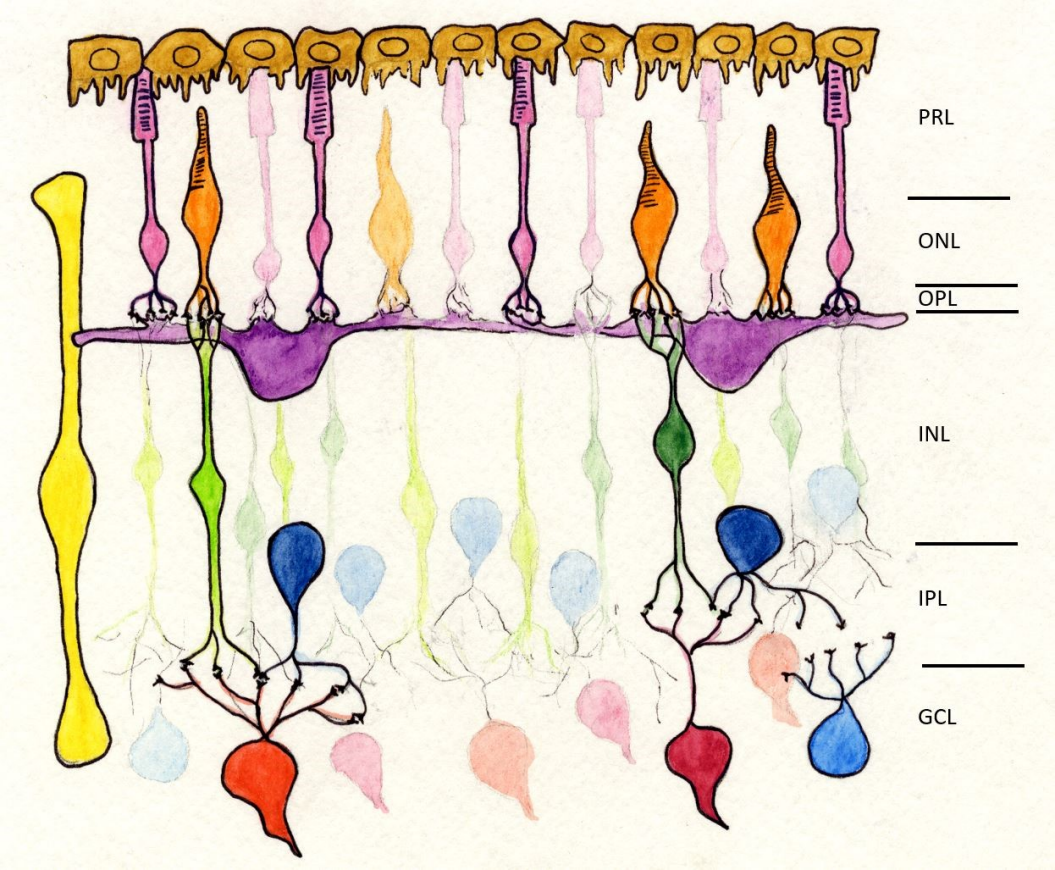

Figure 1.1: Schematic of the retina. Retinal pigmented epithelium (brown) lines the back of the eye, and are directly adjacent to the photoreceptor layer (PRL) that contains the outer segments of rods (pink) and cones (orange). The outer nuclear layer (ONL) contains cell bodies of photoreceptors. Synapses between photoreceptors, bipolar cells (green) and horizontal cells (purple) are located in the outer plexiform layer. Cell bodies of horizontal, bipolar and amacrine (blue) cells are located in the inner nuclear layer (INL). Synapses between amacrine cells, bipolar cells and ganglion cells (red) are located in the ganglion cell layer. Müller cells (yellow) run radially from the ONL to the GCL. In bipolar cells and ganglion cells, ON pathways are illustrated with lighter colours, and OFF pathways are illustrated in darker colours.

the optic disc and projecting to visual relay centers in the brain (Wässle, 2004; Sanes and Zipursky, 2010; Dowling, 2012; Masland, 2012).

In the absence of light, photoreceptors are in a state of constant depolarization maintained by ion flux through cyclic nucleotide gated ion channels in the outer segment membrane (Hagins et al., 1970; Stryer, 1986). This results in the sustained release of the excitatory neurotransmitter glutamate from the photoreceptor terminals into the OPL. Light from the external environment is detected by the photoreceptor outer segments. Rod outer segment disc membranes contain rhodopsin, a G-protein coupled receptor able to detect photons (Palczewski et al., 2000). When a photon arrives, it catalyzes the conversion of 11-*cis*-retinal into all-*trans*-retinal. This photoisomerization event causes the α subunit of the heterotrimeric G-protein transducin (T_α) to dissociate from the βγ subunits ($T_{\beta\gamma}$), consequently activating T_α. Activated T_α binds to the regulatory subunit of phosphodiesterase (PDE), allowing the catalytic subunit to degrade cyclic guanosine monophosphate (cGMP) (Stryer, 1986). This drop in cytosolic cGMP causes the closure of the channels, which decreases the ion flux across the outer segment membranes and hyperpolarizing the cell (Fesenko et al., 1985). Hyperpolarization results in less glutamate being released into the synaptic space (Bloomfield and Dowling, 1985).

Simply put, visual information is passed from the photoreceptors to bipolar cells, and then to RGCs. RGCs fire action potentials (APs) in response to the visual signal. This vertical information flow is divided broadly into two distinct pathways: the ON pathway and the OFF pathway (Werblin and Dowling, 1969; Kaneko, 1970; Dacey et al., 2000). The OFF pathway is a sign-conserving pathway. OFF bipolar cell dendrites contain the α-amino-3-hydroxy-5-methyl-4-isoxazole propionic acid (AMPA) and kainate ionotropic

glutamate receptors, which are non-selective cation channels. Upon binding of glutamate, these receptors open their pores and allow cations ions to flow in, depolarizing the bipolar cell (Shiells et al., 1981; Slaughter and Miller, 1983). The light-induced reduction of glutamate causes the channels to close, hyperpolarizing the bipolar cell reducing glutamate release onto RGCs. Therefore, at the level of the RGC, APs are discharged in response to decreases in illumination. In contrast, the ON pathway is sign-inverting, and ON bipolar cells dendrites express a metabotropic glutamate receptor mGluR6 (Nawy, 1999). This receptor is coupled to an inhibitory G-protein. Through a series of intracellular second messengers, activation of this receptor results in hyperpolarization of the bipolar cell when glutamate is present due to closure of transient receptor potential channels (Shen et al., 2009). Therefore, the light-induced reduction in glutamate leads to the depolarization of the bipolar cell and subsequent neurotransmitter release onto RGCs. ON RGCs fire APs in response to increases of illumination. Visual information is also processed laterally by horizontal cells and amacrine cells. Horizontal cells are interneurons that synthesize and release γ-aminobutyric acid (GABA), whose dendrites contact cone pedicles and whose axons contact rod spherules (Lam et al., 1978; Wässle, 2004). From this position, they are ideally suited to integrate light responses of multiple photoreceptors across large fields, mediating critical processing functions including lateral inhibition. Amacrine cells are a diverse population of retinal neurons that are responsible for lateral processing of the visual signal between bipolar cells and RGCs.

This model becomes immensely complicated when we consider the different subtypes of each cell type. It is well documented that each cell type in the retina contains multiple anatomical and functional subtypes. In the mammalian retina, two types of

horizontal cells, 12-13 types of bipolar cells, >22 types of amacrine cells, and >32 types of RGCs have been documented (Müller and Peichl, 1993; Peichl and González-Soriano, 1994; MacNeil and Masland, 1998; Paus et al., 2003; MacNeil et al., 2004; Wässle et al., 2009; Baden et al., 2016). The diverse populations within each cell type leads to a multitude of connectivity patterns and response profiles generated to encode every aspect of the visual world, and consequently form the basis of the complex visual perception we experience.

1.2 Retinal Ganglion Cell Injury and Animal Models

There are many pathological conditions that result in vision loss. A recent systematic review conducted by the Vision Loss Expert Group of the Global Burden of Diseases, Injuries and Risk Factors Study estimated that 34.2 million (0.5% if the global population) people were clinically blind (presenting best visual acuity < 3/60), and an additional 191 million (2.3% of the global population) had moderate to severe visual impairment (presenting best visual acuity between 6/18 and 3/60 (Stevens et al., 2013)). Though pathological mechanisms of visual disorders differ widely, a common feature of many blinding conditions is the degeneration of RGCs. RGC degeneration is detrimental to vision, as it results in the loss of connection between the retina and the brain, preventing higher order visual processing and visual perception. Two of the most common visual disorders involving RGC death are glaucoma and diabetic retinopathy, that together account for 3% (2% glaucoma; 1% diabetic retinopathy) of the global incidence of visual impairment, and 9% (8% glaucoma; 1% diabetic retinopathy) of the global incidence of blindness in 2010 (Pascolini and Mariotti, 2010).

Just as pathological mechanisms leading to overall vision loss vary widely in

different conditions, of those with RGC involvement, the underlying pathology leading to RGC death differ as well. For example, in glaucoma the defining pathological hallmark is significant damage to the optic nerve head, resulting in the loss of RGCs (Foster et al., 2002). In contrast, diabetic retinopathy results from hyperglycemia-induced breakdown of the blood-retinal barrier that leads to RGC death (Barber et al., 1998; Antonetti et al., 2012). In elucidating specific mechanisms leading to the development and progression of retinal pathology, animal models have proven invaluable.

Many animal models have been developed to study various ocular diseases, however RGC death is often studied using the optic nerve transection (ONT or axotomy) model. In this model, experimental animals (typically mice or rats) undergo surgery to completely transect the optic nerve. This results in vision loss caused by degeneration of RGCs (Quigley et al., 1977; Berkelaar et al., 1994; Nadal-Nicolás et al., 2015). Many processes have been implicated in the death of RGCs following ONT; including, but not limited to, the loss of trophic support and responsiveness to trophic factors (Berkelaar et al., 1994; Shen et al., 1999), excitotoxicity (Russelakis-Carneiro et al., 1996; Yoles and Schwartz, 1998; Kikuchi et al., 2000), oxidative stress (Lieven et al., 2006; Kanamori et al., 2010), and endoplasmic reticulum (ER) stress (Hu et al., 2012). These processes are not unique to RGC damage induced by axotomy, but are hypothesized to play a role in RGC death in various conditions including glaucoma and diabetic retinopathy (Zhang et al., 2000; Li and Puro, 2002; Ng et al., 2004; Tezel et al., 2005; Holcombe et al., 2008; Munemasa et al., 2009; Santiago et al., 2009; Chidlow et al., 2011; Cueva Vargas et al., 2015). Therefore, ONT represents a good model to study RGC cell death mechanisms.

1.3 Calcium

In most neurons, calcium is a widely used second messenger molecule that is able to modulate a multitude of important cellular functions. The concentration of free intracellular calcium ions ($[Ca^{2+}]_i$) is maintained at <50 nM (compared to >1 mM extracellularly). To maintain this large gradient across the cell membrane, various processes are in place to ensure tight $[Ca^{2+}]_i$ regulation. Excess Ca^{2+} ions are extruded from the cytosol into the extracellular environment by the plasma membrane Ca^{2+} ATPase, or the Na^+/Ca^{2+} exchanger (Brini and Carafoli, 2011). Furthermore, Ca^{2+} is sequestered into the ER, and to a lesser extent the mitochondria (Markram et al., 1995; Babcock et al., 1997). Numerous Ca^{2+}-binding proteins, such as calmodulin and calcineurin, are also present in the cytoplasm which help to buffer Ca^{2+} levels as well as contribute to intracellular signaling cascades (Brini et al., 2014).

As mentioned, Ca^{2+} is involved in a multitude of important neuronal cellular functions (for extensive review, see Brini et al., 2014). For example, K^+ currents arising through Ca^{2+}-activated K^+ channels play a role in the repolarization and afterhyperpolarization phases of APs in both projection neurons and interneurons of various brain regions, thus affecting the shape of the AP and the firing frequency, respectively (Shao et al., 1999; Faber and Sah, 2002; Edgerton and Reinhart, 2003; Goldberg and Wilson, 2005). Additionally, release of neurotransmitters from the axon terminal following an AP is Ca^{2+}-dependent (Lev-Tov and Rahamimoff, 1980). Calcium enters the nerve terminal through voltage-gated Ca^{2+} channels (VGCC) that open upon membrane depolarization and, once in the terminal, Ca^{2+} interacts with synaptotagmin, a Ca^{2+} sensor critically important in the final steps of vesicle fusion with the plasma

membrane resulting in neurotransmitter release (Bommert et al., 1993; Littleton and Bellen, 1995; Zimmerberg et al., 2006). Furthermore, activity-dependent Ca^{2+} dynamics, mediated by both ionotropic and metabotropic neurotransmitter receptors, are involved in the regulation of gene transcription by activating nuclear signaling pathways (e.g. mitogen activated protein kinase pathway) as well as by facilitating the interaction between the cyclic AMP response element and its various regulatory binding proteins (Deisseroth et al., 1998; Hu et al., 1999; Dolmetsch et al., 2001; Hardingham et al., 2001). As Ca^{2+} is a critically important second messenger, it's regulation is of utmost importance in maintaining neuronal function and survival.

1.3.1 Pathological Role of Ca^{2+}

It is well documented that Ca^{2+} can be detrimental to cell survival. Evidence that Ca^{2+} influx is involved in cell death arose from early studies showing that extracellular Ca^{2+} is required for toxin-induced death of hepatocytes and agonist-induced cell death in myocytes (Leonard and Salpeter, 1979; Schanne et al., 1979). Major changes in Ca^{2+} homeostasis and Ca^{2+} signaling, and Ca^{2+}-dependent processes, have since been implicated in both triggering and modulating cell death pathways. Two important and well-characterized cell death processes are apoptosis and necrosis. Apoptosis is the most studied form of programmed cell death, whereby a cell executes a specific genetically controlled program that leads to death. This process is critically important in development and turnover in regenerative tissues, and can also be triggered by damaging stimuli (Kerr et al., 1972). Apoptosis is triggered by the activation numerous signaling pathways that activate caspases, proteins in the cysteine protease family, which trigger molecular events leading to the progression of apoptosis (reviewed by Orrenius et al.,

2004). Morphologically, apoptosis occurs in two stages. First, cytoplasmic and nuclear matter is condensed, the nucleus fragments, and the membrane undergoes blebbing to form apoptotic bodies that contain cellular constituents including organelles and nuclear material. Second, apoptotic bodies are rapidly phagocytosed by neighbouring cells or macrophages and degraded in phagosomes and lysosomes (Kerr et al., 1972). Necrosis involves converging signaling pathways that culminate in membrane permeabilization, causing severe cell swelling, loss of membrane integrity, membrane rupture and cell lysis (Proskuryakov et al., 2003). Ca^{2+} plays an integral role in both of these forms of cell death, and may be involved in RGC death in ONT.

Three hypothesized causes of RGC death in ONT include loss of trophic support from target structures, excitotoxicity and oxidative stress. Cytoplasmic and mitochondrial Ca^{2+} overload, as well as ER Ca^{2+} dysregulation are known cell-death triggers as well as likely downstream effects of these stressors. For example, cytosolic Ca^{2+} is sequestered into the mitochondria by the mitochondrial Ca^{2+} uniporter that increases conductance in response to sustained elevations of cytosolic [Ca^{2+}], as would occur in excitotoxicity (Choi, 1994; Babcock et al., 1997; Kirichok et al., 2004). Inside the mitochondrial membrane, pathologically increased [Ca^{2+}] is able to trigger the opening of the permeability transition pore (PTP), a milestone in both apoptosis and necrosis progression (Qian et al., 1999; Pan et al., 2014). Once open, the PTP allows the displacement of cytochrome C from the mitochondria to the cytosol, where it activates caspase cascades (Orrenius et al., 2003). Therefore, increased levels of cytosolic and mitochondrial Ca^{2+} levels can trigger cell death pathways via the formation of the PTP. Cytosolic Ca^{2+} levels can also rise due to the entrance of ions from the extracellular space

during neuronal stimulation, as well as from the release of ions from the ER. Additionally, the interaction between oxidative stress and Ca^{2+} dysregulation is well documented (reviewed in Ermak and Davies, 2002). In a simple model, reactive oxygen species (ROS) are capable of stimulating Ca^{2+} release from the ER by promoting activation of the inositol-trisphosphate receptor on ER membranes (Graier et al., 1998). Therefore, potentially triggering cytoplasmic Ca^{2+}-mediated death pathways. Additionally, if the ER Ca^{2+} pool drops too much, this can trigger errors in protein folding and ER stress (Orrenius et al., 2003). Consequently, if ER stress remains elevated, it can trigger cell death pathways to eliminate the cell. These relatively simple models of how Ca^{2+} is involved in triggering cell death pathways in response to stressors are only two examples of many processes involving numerous other modulatory proteins that play important roles in cell survival. Therefore, researching the role of Ca^{2+} signaling in damaged neural tissue is of immense interest.

1.4 Monitoring Intracellular Ca^{2+} Dynamics

As detailed in the previous sections, Ca^{2+} plays a fundamental role in many physiological and pathological cellular mechanisms. Therefore, the ability to monitor intracellular Ca^{2+} dynamics has proven very useful in studying Ca^{2+}-related cellular activities. Importantly, monitoring Ca^{2+} dynamics in damaged neurons prior to cell death gives important insights into their functional abilities in damaged tissue. A variety of optical methods for imaging Ca^{2+} in cells have been developed. Calcium indicators are fluorescent molecules that are able to bind free cytosolic Ca^{2+}, and change their spectral properties in response (Tsien, 1980; Paredes et al., 2008). Two main classes of calcium indicators are chemical calcium indicator dyes, and genetically encoded Ca^{2} indicators

(GECIs).

1.4.1 Chemical Ca^{2+} Indicators

Chemical Ca^{2+} indicators are engineered molecules with a basic structure derived from known Ca^{2+} chelators, such as EGTA or BAPTA, coupled to a fluorophore (Tsien, 1980; Grynkiewicz et al., 1985; Minta et al., 1989). These molecules change their conformation in response to Ca^{2+} binding, consequently altering the level of fluorescence emitted by the fluorophore. Variability in spectral properties and Ca^{2+} affinity arise from modifications to this base molecule. Quin-2 was the first indicator dye used in biological experiments, but over the years it has been replaced by superior molecules, including fluo-4 and fura-2 (Tsien et al., 1982; Paredes et al., 2008).

Fluo-4 is a popular and widely used single wavelength Ca^{2+} indicator dye, meaning the chromophore is excited by, and emits a single maximum peak wavelength (488 nm excitation; 516 nm emission; Gee et al., 2000). Single wavelength dyes are useful when methodological constraints of additional optical techniques generate the possibility of spectral overlap with other fluorophores (Paredes et al., 2008). Additionally, fluo-4 and other members of its family were developed specifically so to have similar spectral properties to fluorescein to allow use with equipment already established in many laboratories (Minta et al., 1989). Fura-2 on the other hand is a ratiometric indicator, and shifts its absorption maximum from 340 nm when Ca^{2+} is bound to 380 nm when Ca^{2+} is unbound at 512 nm emission. Measurements are obtained by taking the ratio of the emission at 340 and 380 nm excitation. Advantages of using ratiometric over single wavelength indicators is that the ratio corrects for differences or changes in dye concentration within a cell (which can arise because of uneven dye

loading, dye leaking from the cell, and changes in cell volume; Grynkiewicz et al., 1985; Paredes et al., 2008).

A major limitation of using chemical Ca^{2+} indicators to image neurons in the retinal GCL is the duration of loading protocols and specificity. Although several methods to load GCL neurons are available, each has limitations. First, acetoxymethyl ester forms of dyes are convenient, as they are hydrophilic and diffuse readily across membranes into cells, where intracellular esterases remove the acetoxymethyl group trapping the dye inside (Paredes et al., 2008). Acetoxymethyl dyes are commonly used *in vitro* and can be used to label GCL neurons in neonate animals. However, in adults, this method fails to label GCL cells, likely due to development of the inner limiting membrane (Wong et al., 1995; Baldridge, 1996; Bansal et al., 2000). Second, loading with high RGC specificity can be achieved using dextran conjugated dyes injected directly into the isolated retina. With this technique, the dye is picked up by the soma of multiple cell types as well as RGC axons relatively quickly at the injection site. Dye is also picked up by axons at the injection site is retrogradely transported back to the soma of cells further away. However, this process requires long incubation periods, ranging from 2-6 hours before imaging can occur (Baldridge, 1996; Hartwick et al., 2004). A third method, optic nerve stump loading, where dye is applied to or injected into the optic nerve stump of an intact eye or eyecup preparation and retrogradely transported to RGC somas, also yields high RGC specificity but again requires longer incubation periods (Sasaki and Kaneko, 2007; Sargoy et al., 2014). Finally, applying brief electric current to the whole eye or the isolated retina (electroporation) to introduce Ca^{2+} dyes offer drastically shorter wait time (~20 min) following introduction of the dye to the retina but

at the expense of RGC specificity (Yu et al., 2009; Daniels and Baldridge, 2010; Briggman and Euler, 2011).

1.4.2 Genetically Encoded Ca^{2+} Indicators

Although chemical calcium indicators have proven extremely useful, recent technological advances led to the development of GECIs. In principle, the design of GECIs is similar to that of chemical indicators, with a Ca^{2+}-binding component coupled to a fluorescent reporter that changes its spectral properties in response to Ca^{2+} binding. The major advantage to using GECIs is the ability to target the indicator to known cell populations using specific promoter sequences. GECI expression within cells should also be long-lasting whereas even the best chemical indicators are eventually lost from cells or vesicularized and no longer exposed to cytosolic Ca^{2+}. Development of transgenic animals that express GECIs obviate the need for the invasive procedures needed to introduce chemical indicators. Long-lasting GECI expression, without the need for invasive procedures, makes the use of transgenic GECI mice ideal for *in vivo* imaging. There are two general groups of GECIs: proteins excited at single wavelength, and fluorescence measured at a single emission wavelength; or proteins that depend on fluorescence (Förster) resonance energy transfer (FRET).

The original GECIs were termed “cameleons” and depended on FRET occurring between two fluorescent proteins in a Ca^{2+}-dependent manner (Miyawaki et al., 1997). This involved a fusion protein containing a blue fluorescent protein (BFP), calmodulin, the M13 domain of myosin light-chain kinase, and a green fluorescent protein (GFP) in serial arrangement. When Ca^{2+} is not present, calmodulin and M13 do not associate and the molecular construct remains linear; when the BFP is excited (370 nm), it emits at 440

nm. When Ca^{2+} is present, calmodulin and M13 associate with one another, which brings the two fluorescent proteins closer together allowing FRET; exciting BFP with 370 nm light results in energy transfer to the GFP, and the fluorescence emitted is that of GFP (510 nm) (Miyawaki et al., 1997). With FRET-based GECIs like the cameleons the ratio between emitted wavelengths provides the same advantages as with ratiometric chemical calcium indicators, most importantly, correction for differences in GECI expression from cell to cell.

Currently the most popular family of single fluorescent protein based GECIs is the GCaMP family. GCaMPs were developed after the realization that GFP is permissible to a circular permutation without completely losing its fluorescence capability (Baird et al., 1999). With this discovery, a circularly permuted GFP (cpGFP) was fused with calmodulin at the C-terminus, and M13 at the N-terminus to make GCaMP (Nakai et al., 2001). With this construct, when Ca^{2+} is not present, M13 and calmodulin do not associate, and the GFP is in a conformation that emits little fluorescence (at 516 nm) when stimulated with the excitation wavelength (488 nm). When calcium is present, calmodulin and M13 associate with one another, leading to a conformational change in the GFP that allows stronger emission when stimulated by the excitation wavelength.

Since the development of the original GECIs, modifications to these initial constructs have been made to alter Ca^{2+} binding affinity, excitation wavelength and brightness (Tian et al., 2009; Horikawa et al., 2010; Zhao et al., 2011; Chen et al., 2013a, 2013b; Muto et al., 2013). The ultimate goal of these modifications was to enhance the sensitivity and speed so that the performance of GECIs are comparable to chemical indicators. The second generation of GCaMP, GCaMP2, had been extensively

characterized and its flaws well documented, including extremely dim baseline fluorescence and low signal-to-noise ratio (Akerboom et al., 2009). When its crystal structure was solved, intelligent design of future generations of the molecule to improve these qualities was possible (Akerboom et al., 2009). GCaMP3 was generated by creating four point mutations in the GCaMP2 construct that conferred brighter baseline fluorescence, higher Ca^{2+} affinity, and a larger dynamic range as compared to its predecessor (Tian et al., 2009). Since the development of GCaMP3, newer generations have been developed, including the widely popular GCaMP6 family. These newer generations exhibit increased Ca^{2+} sensitivity, faster kinetics, and lower baseline fluorescence resulting in a larger dynamic range and the ability to detect Ca^{2+} transients at a sub-AP threshold (Chen et al., 2013a; Ding et al., 2014). However, the increased baseline fluorescence while still maintaining an acceptable dynamic range characteristic of GCaMP3 makes it the ideal candidate for *in vivo* Ca^{2+} imaging, as it is visible at low levels of $[Ca^{2+}]_i$ and still increases drastically with activity-dependent changes in $[Ca^{2+}]_i$.

1.5 Expressing GECIs in RGCs

There are multiple techniques to introduce genetic constructs into the retina of experimental mouse models, including virus-mediated transfection, electroporation and the generation of transgenic lines. Adeno-associated virus (AAV)-mediated gene transfer has been used to introduce GCaMP3 into the primary motor cortex of mice for *in vivo* calcium imaging (Tian et al., 2009). In this method, AAV vector plasmids containing the gene of interest (GCaMP3) in the place of viral genes, are injected locally into the brain of the mouse. Inside the cells of the brain, the gene of interest is expressed using host transcription and translation machinery (Weitzman and Linden, 2011). AAV-mediated

gene delivery is a well-known concept in retina research; AAV-mediated gene therapy for genetic degenerative retinal conditions has been prevalent in the literature for many years now (for review see Schön et al., 2015). These techniques can easily be reproduced to introduce GCaMP and other GECIs to retinal cells. A second approach to retinal gene delivery is *in vivo* electroporation (Dezawa et al., 2002; Matsuda and Cepko, 2004; Nickerson et al., 2012). In this method genetic constructs are introduced into the eye of an anesthetized mouse by intravitreal injection for targeting cells in the inner retina, or by subretinal injection for cells in the outer retina. Immediately following injection, the entire eye globe is electroporated to introduce the genetic material into the cells. This method has been used to successfully deliver constructs into RGCs, and therefore also has the potential in introducing GECIs (Dezawa et al., 2002). Finally, transgenic mouse lines can be created by delivering the GCaMP gene and associated promoters directly into the pronuclei of fertilized oocytes (Díez-García et al., 2005; Chen et al., 2012). These oocytes are then transplanted into a pseudopregnant foster mother, and carried to term. Transgenic progenies are then generated and maintained by inbreeding of positive genotypes. With this technique, inserted genes are expressed in the entire organism, and provided the promoter included is expressed in RGCs, retinal expression will occur. This technique was used to develop the Thy1-GCaMP3 transgenic mouse line, the animal model studied in this thesis.

1.6 Thy1-GCaMP3 Transgenic Mouse

Chen and colleagues (2012) generated a transgenic mouse line that expresses GCaMP3 under control of the Thy1 promoter. The group generated six founder lines, and continued breeding from the line that exhibited the strongest expression in the CNS and is

commercially available from Jackson Laboratories (B6;CBA-Tg(Thy1-GCaMP3)6Gfng/J, Stock # 017893). Transgenic animals are born at a rate following Mendelian genetics, and are behaviourally and histologically normal (Chen et al., 2012). In these animals, GCaMP3 is widely expressed primarily in excitatory projection neurons of numerous brain regions. GCaMP3 is distributed in the cytoplasm of the soma and neurites, but not in the nucleus, and this expression is maintained longitudinally (Chen et al., 2012).

Functionally, GCaMP3 expressed in these animals was able to reliably report spontaneous intracellular calcium transients in cortical layer V neurons that correlated well with spontaneous spike activity measured by cell-attached recording in acute brain slices (Chen et al., 2012). Furthermore, evoked APs elicited changes in fluorescence intensity that were well correlated to the number of APs. At a population level, bath application of high K^+ solution was able to elicit robust and dramatic increases in GCaMP3 fluorescence. Additionally, these results were replicated in *in vivo* preparations, where robust Ca^{2+}-mediated GCaMP3 activation was correlated with motor activity in awake, behaving mice. This was also the case in brain regions of sensory systems; whisker stimulation elicited Ca^{2+} responses in the corresponding barrel field cortex, and odorant presentation elicited large and spatially distinct patterns of Ca^{2+} responses in glomeruli (Chen et al., 2012). These results indicated that GCaMP3 expression in these transgenic animals allowed the recording of neuron activity in response to stimulation at a single-cell and population level in both *in vitro* and *in vivo* preparations.

1.7 Hypothesis and Objectives

Our laboratory has an interest in developing an *in vivo* Ca^{2+} imaging system to

monitor longitudinal changes in Ca^{2+} dynamics in order to better understand the mechanisms by which Ca^{2+} contributes to long-term changes in RGC dysfunction in degenerative retinal diseases. The Thy1-GCaMP3 transgenic mouse line stood out as an ideal animal model to begin such experiments with for several reasons. First, the genetic expression of the Ca^{2+} reporter in CNS projection neurons eliminates the need for invasive and technically challenging labeling procedures, such as intraocular injections or electroporation. Second, the high baseline fluorescence and large dynamic range exhibited by GCaMP3 would permit imaging of RGCs at rest before beginning the stimulus, and then obtain robust increases of fluorescence when stimulated. Third, the stable genetic expression of the Ca^{2+} indicator allows imaging of the same population of RGCs repeatedly in longitudinal experimental designs.

This transgenic mouse line has been well characterized and used in research in the brain, spinal cord, and peripheral nervous system (Chen et al., 2012; Adam et al., 2014; Vazquez et al., 2014; Gao et al., 2015; Tang et al., 2015; Wang et al., 2016a). This line has the potential to be a valuable tool for studying RGC Ca^{2+} dynamics in normal and pathological conditions; however, very little is known about its anatomical distribution and performance in the retina. Published data on the anatomical distribution of GCaMP3-expressing cells in the retina is extremely limited and to our knowledge, there have been no published functional studies of Thy1-GCaMP3 expressing retinal neurons.

The Thy1 promoter has been used in the past to generate transgenic mice lines expressing various fluorescent proteins in excitatory projection neurons (Feng et al, 2000). Two of these lines, Thy1-CFP(23) and Thy1-YFP(H) have been used in retina research. Characterization in the retina of these animals indicates that many

immunolabeled RGCs indeed expressed the fluorescent protein; however, fluorescence was also detected in cholinergic and GABAergic displaced amacrine cells in the GCL (Raymond et al., 2008; Wang et al., 2010). Furthermore, following optic nerve injury, CFP fluorescence was detected in microglia after phagocytosis of dead RGCs, which can obstruct RGC imaging (Wang et al., 2010). Additionally, blood-retinal-barrier disruptions have been shown to quench the YFP fluorescence signal in a model of optic nerve trauma suggesting that damage can affect the function of fluorescent proteins (Wang et al., 2011). Taken together, these results suggest that the Thy1 promoter does not always drive expression uniquely to RGCs, and that changes to exogenous protein distribution and fluorescence reporting capabilities can be altered with axonal injury. Therefore, characterization of the distribution of GCaMP3 and its functional abilities in the retina in the absence and presence of tissue injury is required prior to adopting this transgenic line as a means to study RGC Ca^{2+} in normal retinas and in models of retinal disease.

Therefore, the purpose of this research was to assess the properties of GCaMP3 in RGCs and to determine if GCaMP3 expression and response to elevated $[Ca^{2+}]_i$ are maintained in a model of RGC damage, optic nerve transection (axotomy). We hypothesize that in Thy1-GCaMP3 transgenic mice GCaMP3 is expressed uniquely in RGCs and persistently reports intracellular Ca^{2+} dynamics under normal conditions, as well as following RGC damage.

Chapter 2: Materials and Methods

2.1 Animals and Tissue Preparation

Protocols were approved by the Dalhousie University Committee on Laboratory Animals, and all procedures performed in accordance with regulations established by the Canadian Council on Animal Care. All chemicals, reagents and solutions were obtained from Sigma-Aldrich (Oakville, ON, Canada) unless otherwise stated, and were prepared fresh in phosphate buffered saline (PBS) from stock solutions or in double distilled water and kept at -20°C, or as per manufacturer's instructions.

Mice used in this study were purchased from Jackson Laboratories (Bar Harbor, ME, USA), and housed at the Carleton Animal Care Facility at Dalhousie University. Thy1-GCaMP3 mice (B6;CBA-Tg(Thy1-GCaMP3)6Gfng/J, Stock # 017893, Jackson Laboratories) served as the experimental group, and non-carrier (NCAR) littermates and wild type C57Bl/6 (Stock #000664, Jackson Laboratories) mice served as controls. Mice were housed (with up to four animals per cage), in a 12h light/dark cycle, and had unlimited access to food and water.

In a subset of animals from each group (Thy1-GCaMP, n=7; NCAR, n=4; C57BL/6, n=8), surgery was performed to transect the left optic nerve 1, 3, 5 or 7 days prior to sacrifice, with the right eye serving as an internal control. Mice were anesthetized with 2% isofluorane inhalation and placed in a stereotaxic apparatus and given 0.1 mg/kg buprenorphine to manage postoperative pain. In order to gain better access to the optic nerve, the conjunctiva was sutured (8-0), and tension was exerted on the suture to rotate the eye downward. To expose the optic nerve, a small (0.5-1cm) incision was made in the

skin above the left eyelid near the supraorbital ridge, then a small cut was made in the supraorbital muscle at the orbital ridge. The underlying intraorbital tissues were teased apart to reach the optic nerve. Once exposed, a small incision was made in the dura of the optic nerve approximately 1 mm behind the eye, and the optic nerve was cut at this location with fine scissors. Following optic nerve transection (ONT), the incision in the muscle was sutured (6-0 absorbable), and the skin was sutured (6-0 non-absorbable). Animals were then allowed to recover on a heating pad for a minimum of 20 hours, prior to their return to regular housing facilities. Animals that underwent ONT were selected for experiments 1, 3, 5 or 7 days after the procedure (Figure 2.1).

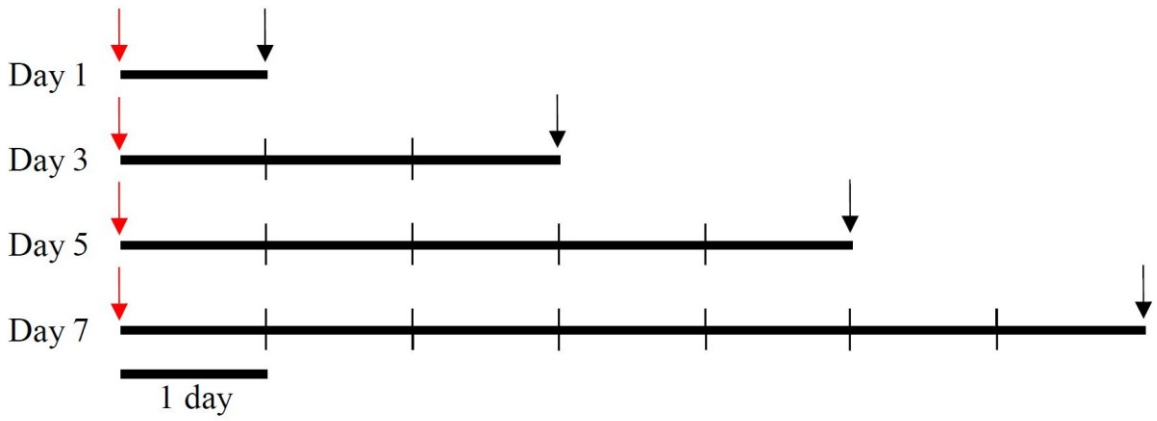

Figure 2.1: Timeline for ONT experimental groups. Red arrow indicates time of ONT surgery, black arrow indicates time of sacrifice and calcium imaging.

At the time of each experiment, animals were sacrificed by lethal intraperitoneal injection of sodium pentobarbital (2.4mg/kg). Eyes were enucleated immediately and placed in room temperature Hibernate A (ThermoFisher, Waltham, MA, USA). RGCs of control mice (both NCAR littermates and C57B6/L mice) were loaded with calcium indicator dye by electroporation. Fura-2 calcium indicator dye (750 nL of 20 mM fura-2 pentapotassium salt solution; Invitrogen, Burlington, ON, Canada) was injected into the enucleated eye through the optic disk with a Hamilton syringe. Tweezertrodes (BTX, Holliston, MA, USA) were positioned on the eye with the cathode on the cornea and square wave pulses (five 10 ms pulses at 30 V) were applied with the ECM 830 electroporation system (BTX). Retinas were carefully isolated by dissection, and vitreous removed by gentle tweezing using forceps. Retinas were cut in half and mounted on black filter paper (Millipore, Billerica, MA, USA) with the GCL facing up. Isolated retinas were maintained in Hibernate A solution for at least 60 minutes, prior to being transferred to a microscope-mounted superfusion chamber for calcium imaging.

2.2 Calcium Imaging

Retina halves were placed in a microscope-mounted superfusion chamber (~ 1 ml volume), and superfused with oxygenated Hank's Balanced Salt Solution (100% O_2, Praxair, Dartmouth, NS; HBSS, 10 mM HEPES, pH 7.4) at a rate of ~ 2ml/min. Retinas were imaged with a charge-coupled device camera (Sensicam PCO, Germany) connected to a Zeiss Axioskop microscope equipped with a 40X water immersion objective (0.80 W numerical aperture, Achroplan; Carl Zeiss Meditec, Oberkochen, Germany) and recorded using Axon Imaging Workbench 4 software (Molecular Devices, Sunnyvale, CA, USA). Images were acquired at a frequency of one frame per 20 seconds, but acquisition was

increased to one frame per five seconds during periods of drug applications. Where ratiometric fura-2 dye (K_d = 224 nM) was used, fluorescence was stimulated using a band-pass filter (XF04 set, excitation 340 or 380 nm; emission 510 nm; dichroic >430 nm; Omega Optical) and image pairs at 340 and 380 nm excitation (510 nm emission) were collected. For Thy1-GCaMP3, fluorescence was simulated using a separate band-pass filter and images were collected at 488 nm excitation (516 nm emission). The effect of kainic acid (KA; Tocris Bioscience, Avonmouth, Bristol, UK) on $[Ca^{2+}]_i$ was tested by bath application of the compound dissolved in 100% oxygenated HBSS (10 mM HEPES, pH 7.4) at various concentrations (10, 50 and 100 μM) for 30 seconds. Each piece or retina was treated three or four times with KA, with at least 15 minutes in between each consecutive application. Following imaging, retinas were prepared for immunohistochemistry.

2.3 Immunohistochemistry

After calcium imaging, retinas were fixed in 4% paraformaldehyde (PFA), in 0.01 M phosphate buffered saline (PBS; 1h at room temperature (RT)). After fixation, retinas were washed with PBS (3 x 30 min at RT). Retinal tissue was blocked with 10% normal donkey serum (Jackson ImmunoResearch Laboratories Inc., West Grove, PA, USA) in PBS (overnight at 4°C), and then incubated for 3-7 days at 4°C in primary antibodies (Table 2.1) diluted in PBS with 0.3% TritonX (PBST). Following incubation in the primary antibodies, retinas were washed in PBS (3 x 30 minutes at RT), and incubated overnight in secondary antibodies diluted in PBST, followed by final washes in PBS (3x30 min at RT). Tissue was mounted on microscope slides using VectaShield (Vector Laboratories, Burlington, ON) mounting medium.

Table 2.1. Primary (1°) and secondary (2°) antibodies.

1° Antibody (Dilution)	1° Manufacturer (catalogue number)	2°Antibody (Dilution)	2° Conjugate Fluorophore	2° Manufacturer (catalogue number)
Guinnea pig anti-RBPMS (1:1000)	PhosphoSolutions (1832-RBPMS)	Donkey anti-guinnea pig (1:1000)	Cy3	Jackson ImmunoResearch (706-165-148)
Goat anti-ChAT (1:100)	Millipore (AB144P)	Donkey anti-goat (1:1000)	Alexa Fluor 633	Invitrogen (A21082)

2.4 Imaging

Tiled images of each hemi-retina were obtained using a Zeiss Axio Imager.M2 microscope, with a 20x Plan-Apochromat objective (0.8 numerical aperture; Zeiss, Oberkochen, Germany), coupled to an Axiocam 506 camera (Zeiss, Oberkochen, Germany) and a 120-watt X-Cite® 120Q excitation light source (Excelitas Technologies, Waltham, MA, USA). GCaMP3, RBPMS and ChAT fluorescence images were acquired using specific beam splitters and band-pass filters for each fluorophore (Table 2.2). Exposure time was adjusted manually for each channel for each tiled image acquired.

Table 2.2. Image acquisition for immunohistochemistry.

Image (fluorophore)	Beam Splitter	Filter excitation range	Filter emission range
GCaMP3	495 nm	450-490 nm	500-550 nm
RBPMS (Cy3)	560 nm	540-552 nm	575-620 nm
ChAT (AlexaFluor 633)	660 nm	620-655 nm	665-715 nm

2.5 Data Analysis

2.5.1 Ca^{2+} Imaging

Using Axon Imaging Workbench 4 (Molecular Devices, Sunnyvale, CA, USA), GCL cells were circled as regions of interest (ROIs) post-hoc. For each ROI, the software measured fluorescence level (GCaMP3) or fluorescence ratio (fura-2) over time. This output was transferred into the ClampFit 10.4 software (Molecular Devices, Sunnyvale, CA, USA). In ClampFit, cursors were used to obtain baseline (F_0) and peak (F) fluorescence change for each drug application. Transient amplitudes were defined as peak fluorescence over baseline (F/F_0). Resting GCaMP3 fluorescence was also obtained by averaging the fluorescence measurements of the first 15 frames for each ROI. Prism6 (GraphPad, La Jolla, CA, USA) was used for graphing and statistical analysis. The data were analyzed by one-way ANOVA followed by Tukey's multiple comparisons test when applicable and data are displayed as mean ± margin of error (ME) for a 95% confidence interval (CI).

2.5.2 Immunohistochemistry

Image analysis was performed using Zen2Lite (Carl Zeiss Meditec, Oberkochen, Germany). The area of each retina was obtained by tracing the area of each hemi-retina using the spline contour graphics tool and adding them together. Retinas had a mean (SD) area of 15.2 (1.9) mm^2. For each retina, ROIs of 500 x 500 µm were selected from the central, middle and periphery of the two quadrants with the best image quality, totaling an area of 1.5 mm^2. These ROIs were exported as individual images and used for cell counting. Based on area measurements of the full retina, counted ROIs represented

9.9 (1.2)% of the full retina area. The number of $GCaMP^+$, $RBPMS^+$, and $ChAT^+$ cells were counted, as well as the number of $GCaMP^+$ cells that were co-labeled with RBPMS or ChAT. For control retinas, descriptive statistics were obtained using Prism6 (GraphPad, La Jolla, CA, USA). Unfortunately, due to the small sample size within each ONT group, statistical analyses of cell counts were not possible.

Chapter 3: Results

The overall objective of the work presented in this thesis was to characterize GCaMP3, a genetically encoded Ca^{2+} indicator, in the retina of the Thy1-GCaMP3 transgenic mouse line. This transgenic animal has proven useful in neuroscience research in the brain and spinal cord, and additionally, has the potential to be extremely valuable in the field of retina research. However, studies examining it's expression and performance in the retina are limited. Therefore, the aim of this work was to fill this gap and determine if this mouse line can be established as a novel approach to study RGC function.

3.1 General Expression Pattern and Function of GCaMP3 in Thy1-GCaMP3 Transgenic Mouse Retinas

The first aim of this project was to determine whether GCaMP3 was uniformly expressed in the retina. Genes inserted using the Thy1 promoter exhibit strong transgene position variation, and transgenic lines often do not show the same expression patterns (Feng et al., 2000). The Thy1-GCaMP3 transgenic line (available commercially from Jackson Laboratories) was chosen because of its high expression level in the brain (Chen et al., 2012); however, whether GCaMP3 is uniformly expressed in retinal tissue was unclear. Figure 3.1 shows that GCaMP3 fluorescence was widely and uniformly observed using fluorescence microscopy in the ganglion cell layer (GCL) of a whole flat-mounted retina (Figure 3.1A, green). Under higher magnification, GCaMP3 fluorescence was observed in the soma cytoplasm and neurites, but not the nucleus, of many neurons in the GCL (Figure 3.1B, green). Triple labeling experiments with antibodies against RNA-binding protein with multiple splicing (RBPMS, red), a specific marker for RGCs

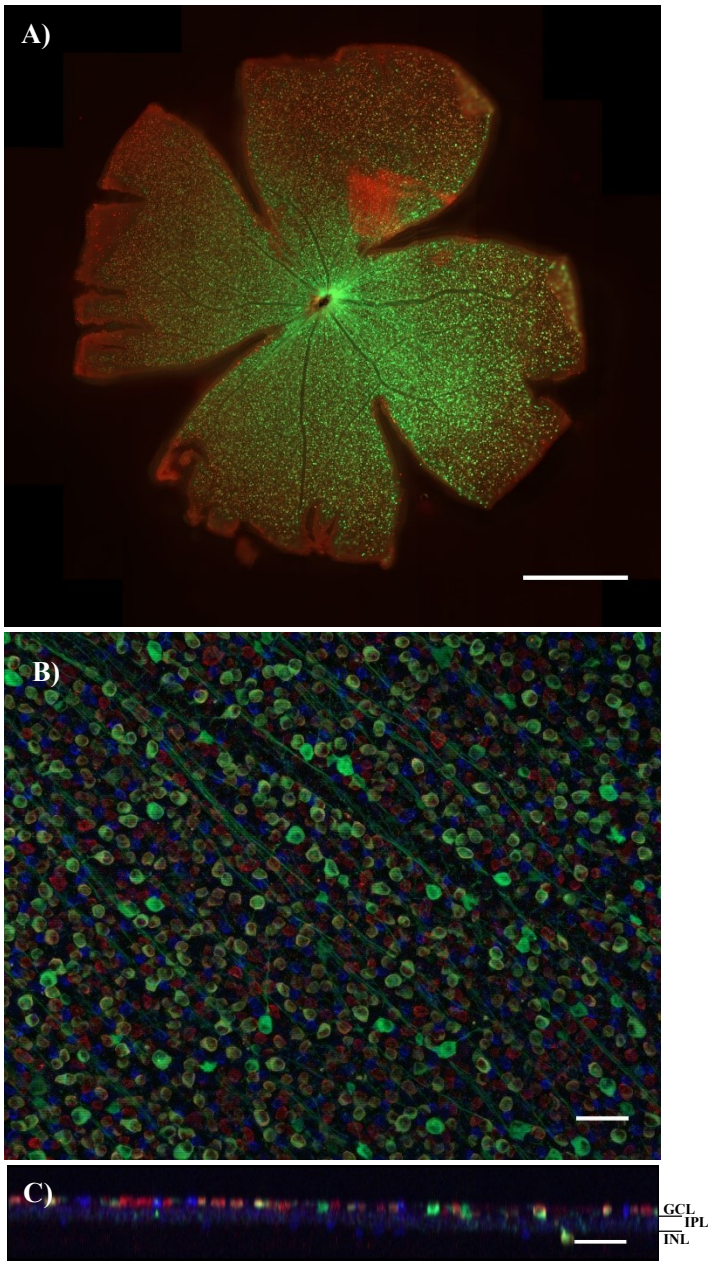

Figure 3.1: Anatomical distribution of GCaMP3 in the retina of Thy1-GCaMP3 transgenic mice. A) Fluorescence micrograph of whole mount retina illustrating widespread expression of GCaMP3 (green) throughout the retina (scale bar = 0.5 mm). **B)** Higher magnification image of a region of Thy1-GCaMP3 retina immunostained with

anti-RBPMS (red) and anti-ChAT (blue) antibodies. GCaMP3 (green) is detected in the soma and neurites, but not in the nuclei of expressing cells (scale bar = 50 μm).
C) Orthogonal projection of the ganglion cell layer (GCL), inner plexiform layer (IPL) and inner nuclear layer (INL) illustrating that GCaMP3 fluorescence is highest in the GCL, but also occurs in displaced ganglion cells in the INL (scale bar = 50 μm).

(Rodriguez et al., 2014), and ChAT (blue), a specific marker for cholinergic amacrine cells, suggests that most GCaMP3$^+$ neurons in the GCL are RGCs. GCaMP3$^+$ cells are also occasionally observed co-localized with RBPMS in the INL, indicating expression by displaced RGCs (Figure 3.1C). Thus, the robust expression of GCaMP3 in the majority of RGCs throughout the retina led us to next investigate the functional properties of GCaMP3.

Superfusion of isolated retinas with kainic acid (KA), an ionotropic (AMPA and kainate) glutamate receptor agonist, reliably reported transient increases of GCaMP3 fluoresence in RGCs, indicative of, and henceforth referred to as, increases in $[Ca^{2+}]_i$ (or simply as "transients" or "transient amplitudes"). As illustrated in Figure 3.2A, increases in $[Ca^{2+}]_i$ from baseline were apparent in response of RGCs to the application of 50 µM KA, with recovery back to baseline following wash. Additionally, there was a concentration-dependent increase in transient amplitude in response to the application of 10 µM, 50 µM and 100 µM KA (Figure 3.2B). These data indicate that GCaMP3 expressed in RGCs is functional, as the protein was able to report increases of the amplitude of Ca^{2+} transients in response to application of increasing concentrations of KA.

We next investigated the impact of RGC injury on the properties of GCaMP3 and KA-induced Ca^{2+} transients in retinas ONT was performed on the left eye of a subset of animals. To ensure that the procedure was successful and selective, RBMPS (to label RGCs) and ChAT (to label cholinergic amacrine cells) immunohistochemistry was performed on retinas following Ca^{2+} imaging experiments. Figure 3.3 shows example photomicrographs depicting that at 7 days post-ONT the density of both GCaMP3$^+$ and

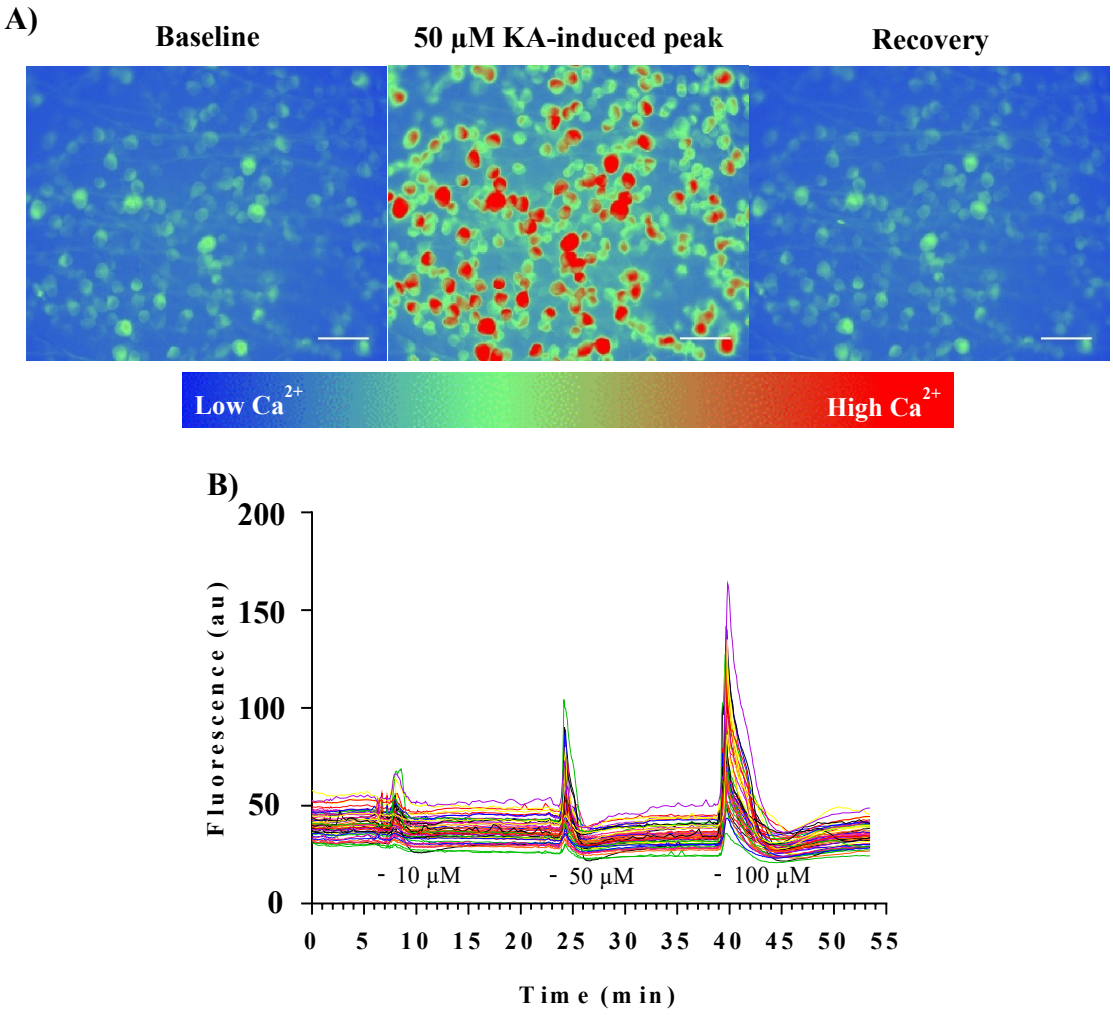

Figure 3.2: Ca^{2+} transients reported by GCaMP3 are robust. A) Pseudocolour photomicrographs taken from Ca^{2+} imaging experiments. Peak change in fluorescence (middle) from baseline (left) in response to elevated $[Ca^{2+}]_i$ induced by bath application of 50 µM KA is evident, returning to baseline (right) after KA is washed out. **B)** Example traces (50 traces selected from one experiment) illustrate that there is a concentration-dependent increase in transient amplitude in response to various KA concentrations. Scale bar = 50 µm.

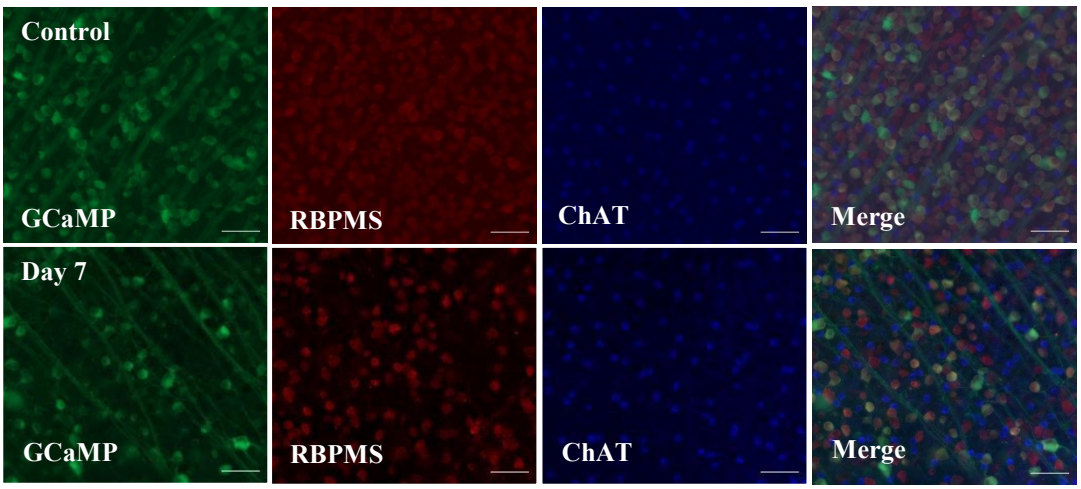

Figure 3.3: RGC density is reduced qualitatively with ONT. Qualitative analysis reveals that in control retinas many GCaMP$^+$ cells were RBPMS$^+$, and that GCaMP was not co-localized with ChAT$^+$ cells. After 7 days post-ONT the density of GCaMP3$^+$ and RBPMS$^+$ cells were reduced and GCaMP3 was still co-localized in many RBPMS$^+$ cells, and not with ChAT$^+$ amacrine cells. Scale bar = 50 μm.

RBPMS$^+$ cells decreased compared to controls, whereas the density of ChAT$^+$ cells was not affected by ONT. Therefore, after ONT GCaMP3 appears to remain expressed in the majority of surviving RGCs.

Ca^{2+} responses to 50 μM KA were quantified in retinas of Thy1-GCaMP3 transgenic mice. Transient amplitudes (measured as peak fluorescence change, F, divided by baseline fluorescence, F_0) of RGCs in ONT eyes were reduced compared to control eyes at each time point (Figure 3.4 and 3.5A). Figure 3.4 shows images of baseline and KA-induced peak fluorescence taken from GCaMP3 Ca^{2+} imaging experiments. In control retinas, 50 μM KA evoked large calcium transients, visible qualitatively as changes of pseudocolour representations from cool to warmer colours, in almost every cell in the field of view, and evident in accompanying representative Ca^{2+} transient traces. Transients 1 day following ONT were slightly reduced compared to control. In contrast, at 3, 5 and 7 days post-axotomy, the same concentration of KA generated only weak responses and many cells did not respond at all. The differences in mean peak Ca^{2+} transient amplitude were quantified and results displayed Figure 3.5A.

After ONT, the mean transient amplitude of GCaMP3-expressing RGCs in response to KA was significantly less in the ONT eye compared to the uninjured fellow eye (Table 3.1, one-way ANOVA, $p<0.05$). Interestingly, not only did mean transient amplitudes decrease compared to control animals in ONT eyes, but transients were also significantly less in fellow eyes of animals that had undergone ONT (one-way ANOVA, $p<0.05$). These data indicate that ONT not only had a significant impact on transient amplitudes evoked by KA in the experimental eyes but also in uninjured fellow eyes. These results demonstrate that GCaMP3 remains in RGCs after ONT and Ca^{2+} transient

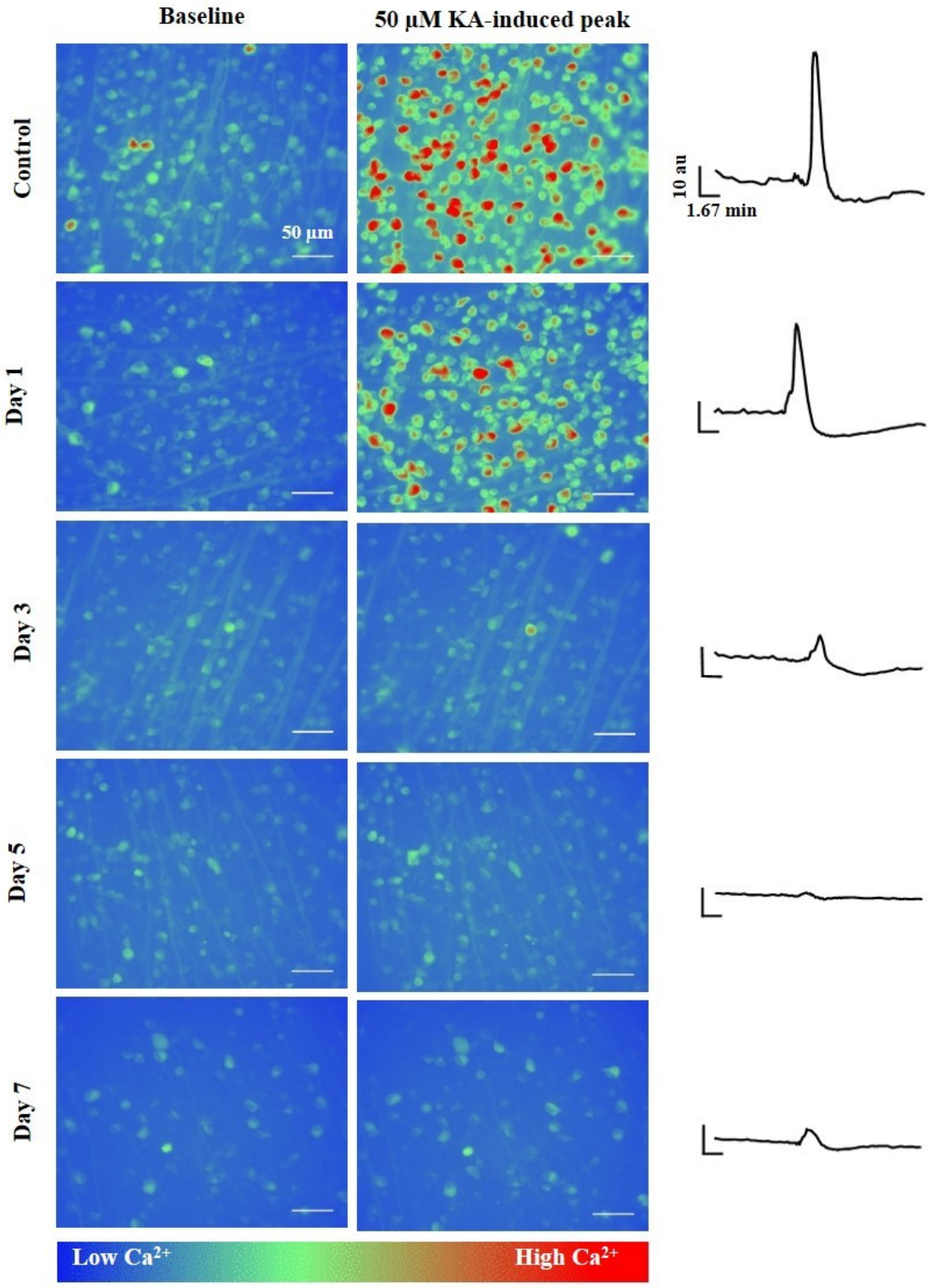
Baseline
50 µM KA-induced peak
Control
Day 1
Day 3
Day 5
Day 7
50 µm
10 au
1.67 min
Low Ca2+
High Ca2+

Figure 3.4: Transient amplitudes decreased after ONT. Example pseudocolour photomicrographs (left: baseline; middle: response to 50 μM KA, scale bar = 50 μm) and example traces (right; horizontal scale bar = 1.67 min, vertical scale bar = 10 au) illustrating increases of Ca^{2+} (GCaMP3 fluorescence) of Thy1-GCaMP3 retinas before (baseline) and at the peak KA-induced fluorescence peak 1, 3, 5 and 7 days after, ONT. With increased time after ONT, measured transient amplitudes were smaller compared to control.

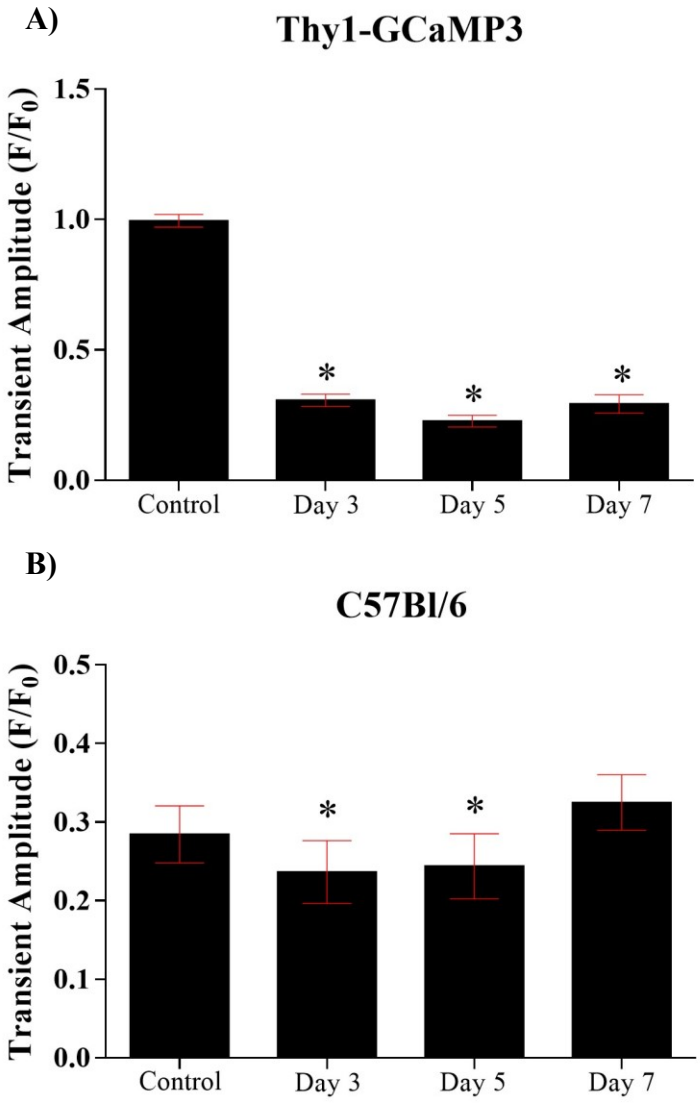

Figure 3.5: Ca^{2+} transients after ONT. A) Transient amplitudes in retinas from Thy1-GCaMP3 transgenic mice reduced significantly 3, 5 and 7 days post-axotomy compared to controls. **B)** Transient amplitudes measured in C57Bl/6 retinas, loaded with fura-2, were reduced 3 and 5 days after ONT, but not 7 days post-ONT compared to control retinas. n= 27-303 cells/experiment, 2-14 experiments/group. *$p<0.05$ compared to controls.

amplitudes were reduced compared to control retinas, which suggests that GCaMP3 may be a useful tool to study cellular changes in RGCs after injury. Thus, we next sought to compare GCaMP3 with results obtained using traditional calcium imaging methods, namely fura-2 loading.

3.2 Comparison of GCaMP3 with Fura-2

Traditional methods to measure $[Ca^{2+}]_i$ typically involve introducing a small molecule dye into the cytoplasm of cells. Fura-2 is a small molecule Ca^{2+} indicator dye that has many advantages, in particular allowing for ratiometric imaging that can correct for differences in dye concentration between cells. However, there are significant limitations to the use of small molecule dyes (see Discussion), which has lead us to examine the Thy1-GCaMP3 mouse. A potential advantage of GCaMP3 over small molecule dyes is that genetic expression of the Ca^{2+} indicator offers ease of use by eliminating the need for challenging and time-consuming loading procedures or techniques, like electroporation, that could affect the integrity of cells. However, it is not clear whether changes in fluorescence measured with GCaMP3 accurately report functional cellular responses, as have been reported previously with small molecule dyes (Baden et al., 2016). Therefore, the second aim of this work was to compare KA-induced Ca^{2+} transients in Thy1-GCaMP3 retinas and Thy1-GCaMP3 non-transgene carrying littermate controls (NCAR) and wild type C57Bl/6 mice whose GCL neurons were loaded with the chemical calcium indicator dye fura-2 by electroporation.

As described above, in Thy1-GCaMP3 retinas, mean transient amplitudes were reduced after ONT (3, 5 and 7 days) compared to control retinas ($p<0.05$; Figure 3.5A). In C57Bl/6 retinas, loaded with fura-2, Ca^{2+} transient amplitudes were significantly

smaller 3 and 5 days after ONT compared to control retinas ($p<0.05$; Figure 3.5B, Table 3.1). Interestingly, 7 days post-ONT, mean transient amplitudes were not significantly different from control retinas (Figure 3.5B, Table 3.1). However, it has been documented that electroporation of calcium indicators into the retina loads both RGCs and displaced amacrine cells in the GCL (Daniels and Baldridge, 2010). Thus, it is possible that experiments conducted 7 days after ONT had a greater number of amacrine cells being measured, which may result in no significant change in Ca^{2+} transient amplitudes, overall, when compared to control retinas. Results using fura-2 in Thy1-GCaMP3 non-transgene carrying littermate control retinas showed a similar pattern (data not shown). Therefore, these results suggest that the genetically encoded Ca^{2+} indicator, Thy1-GCaMP3 may be superior to small molecule dyes due to the specific expression in RGCs, even after axonal injury. However, further characterization of GCaMP3 in the absence and presence of physiologic perturbations is required to ensure changes in detected fluorescence are due to cellular changes and not changes related to the GCaMP molecule itself. Thus, our next goal was to further investigate the functional responses of Thy1-GCaMP3 retinas after ONT.

Table 3.1 Transient amplitudes evoked by 50 μM KA in Thy1-GCaMP3 and C57Bl/6 retinas in control, ONT and fellow eye retinas. Data are represented as mean ± ME (for a 95% confidence interval), One-way ANOVA *$p<0.05$ compared to control

	Transient Amplitude (mean ± ME)						
		Day 3		**Day 5**		**Day 7**	
Group	**Control**	**ONT**	**Fellow**	**ONT**	**Fellow**	**ONT**	**Fellow**
GCaMP3	0.99±0.02	0.31±0.02*	0.79±0.03*	0.23±0.02*	0.59±0.04*	0.29±0.04*	0.49±0.03*
C57Bl/6	0.33±0.03	0.24±0.04*	0.17±0.02*	0.24±0.04*	0.28±0.02	0.33±0.04	0.29±0.03

3.3 Characterization of GCaMP3 transients after ONT

We next sought to further characterize the changes in transient amplitudes evoked by KA in retinas from eyes that had undergone ONT. The initial step in the characterization of GCaMP3 transients after ONT was to determine whether baseline fluorescence reported by GCaMP3 changes after ONT. If so there would be the possibility that axonal injury alters GCaMP3 expression level or modifies the protein's ability to reliably report $[Ca^{2+}]_i$. Qualitatively, photomicrographs taken at baseline from Ca^{2+} imaging experiments indicated that baseline fluorescence of GCaMP3 remained stable following ONT (Figure 3.4, left). To quantitatively determine whether resting fluorescence values reported by GCaMP3 changed in retinas subjected to ONT, GCaMP3 fluorescence measurements of the first 15 images obtained from each experiment were averaged to obtain resting fluorescence values. Using these measurements, the baseline value of all cells in one experiment were averaged to obtain a baseline fluorescence level per experiment. It was determined that mean resting fluorescence emitted by GCaMP3 in control retinas (45.29 ± 6.02 au) was no different than mean resting fluorescence in retinas of eyes that had undergone ONT (Figure 3.6; Day 1: 39.89; Day 3: 39.88 ± 9.55; Day 5: 36.85 ± 3.45; Day 7: 31.55 ± 10.35; one-way ANOVA, $p>0.05$ compared to controls). These data indicate that GCaMP3 fluorescence under resting conditions remained stable following ONT. This is indirect evidence that expression level and reporting capabilities of GCaMP3 is unaltered following ONT.

Following the determination that GCaMP3 fluorescence under basal conditions remained stable after ONT, the next aim was to determine how transient amplitudes change with ONT in response to increasing concentrations of KA. At 1 day post-ONT,

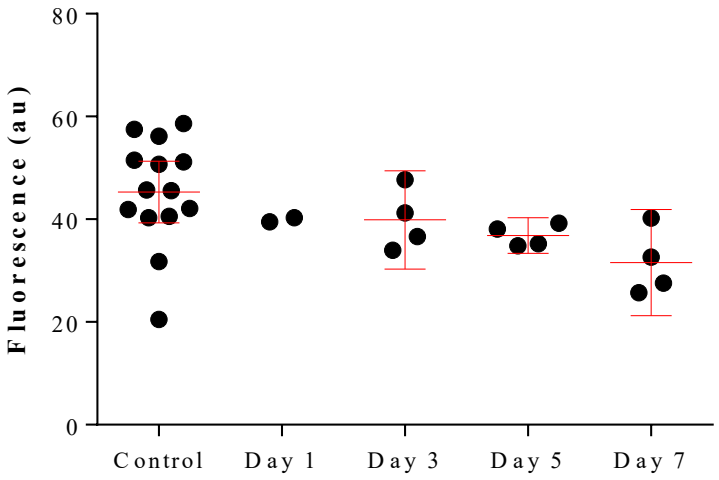

Figure 3.6: Baseline fluorescence reported by GCaMP3 did not change with ONT. Each symbol represents the mean baseline fluorescence of all cells imaged in one experiment (number of cells ranged from 74 at 7 days post ONT to 303 in control). There was no significant difference observed at any time point compared to control.

transient amplitudes evoked by increasing concentrations of KA were inconsistent (Figure 3.7). Mean transients evoked by 50 μM KA were significantly reduced compared to controls (Table 3.2, one-way ANOVA $p<0.05$, compared to controls); however, mean responses to 10 μM KA and 100 μM were significantly larger compared to controls (Table 3.2, one-way ANOVA, $p>0.05$ compared to controls). In contrast, mean transient amplitudes reported by GCaMP3 were consistently and significantly reduced 3, 5 and 7 days post-ONT at all concentrations of KA tested (one way-ANOVA, $p<0.05$, compared to control; Figure 3.8 and Table 3.2).

Table 3.2 Transient amplitudes evoked by KA (ME = margin of error for a 95% confidence interval). *$p<0.05$ compared to control

Concentration	**Transient Amplitude (mean ± ME)**				
	Control	**Day 1**	**Day 3**	**Day 5**	**Day 7**
10 μM	0.15±0.02	0.25±0.03*	0.05±0.01*	0.03±0.01*	0.01±0.01*
50 μM	0.99±0.02	0.88±0.05*	0.31±0.02*	0.23±0.02*	0.29±0.04*
100 μM	1.29±0.04	1.68±0.05*	0.53±0.02*	0.50±0.05*	0.47±0.04*

When conducting the calcium imaging experiments, not only were transient amplitudes reduced after axotomy, but there were also a large number of cells within the field of view that did not appear to respond to KA at all (Figure 3.4). Therefore, to determine whether all GCaMP3$^+$ cells have functional responses, the number of cells that responded to KA were counted for each time point. Cells that exhibited a change greater than 10% of baseline ($F/F0*100>10$) were considered responders (summarized in Table 3.3). Figure 3.9 shows the relative proportions of cells deemed to be responders for each

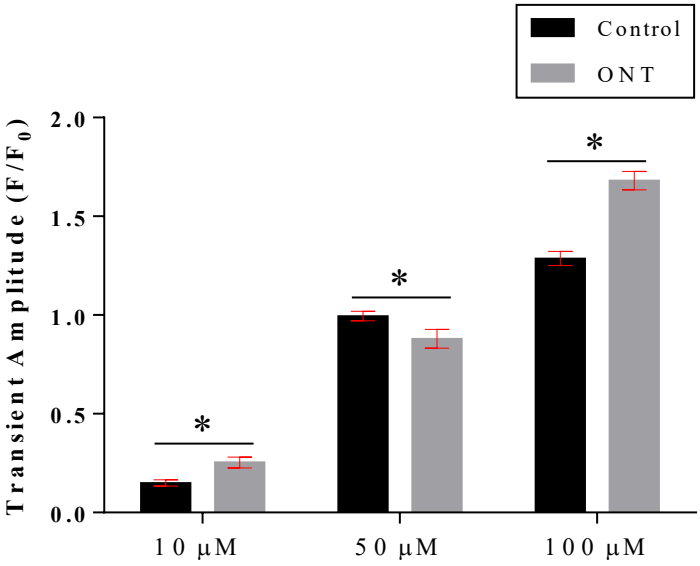

Figure 3.7: Transient amplitudes at one day post-ONT were variable. Transient amplitudes evoked by 10, 50, and 100 µM KA were different but not in a consistent direction one day post-ONT compared to controls. *p<0.05 compared to controls.

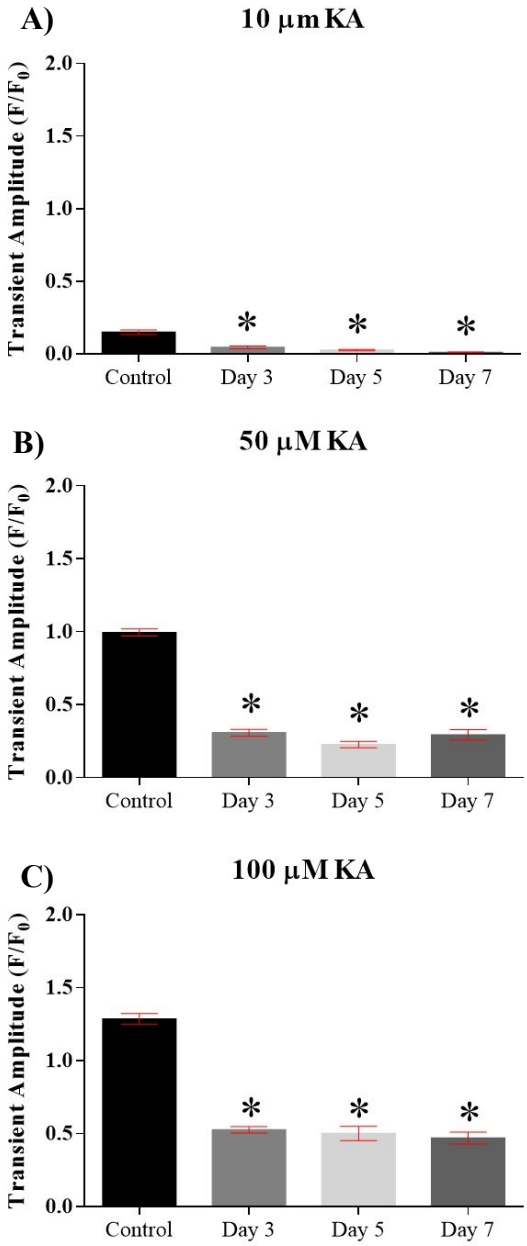

Figure 3.8: With increased time after ONT, Ca^{2+} transient amplitudes were significantly reduced compared to control retinas. Ca^{2+} transient amplitudes in RGCs were significantly lower 3, 5, and 7 days post-ONT compared to controls when evoked by **A)** 10 µM, **B)** 50 µM and **C)** 100 µM KA. *$p<0.05$ compared to control.

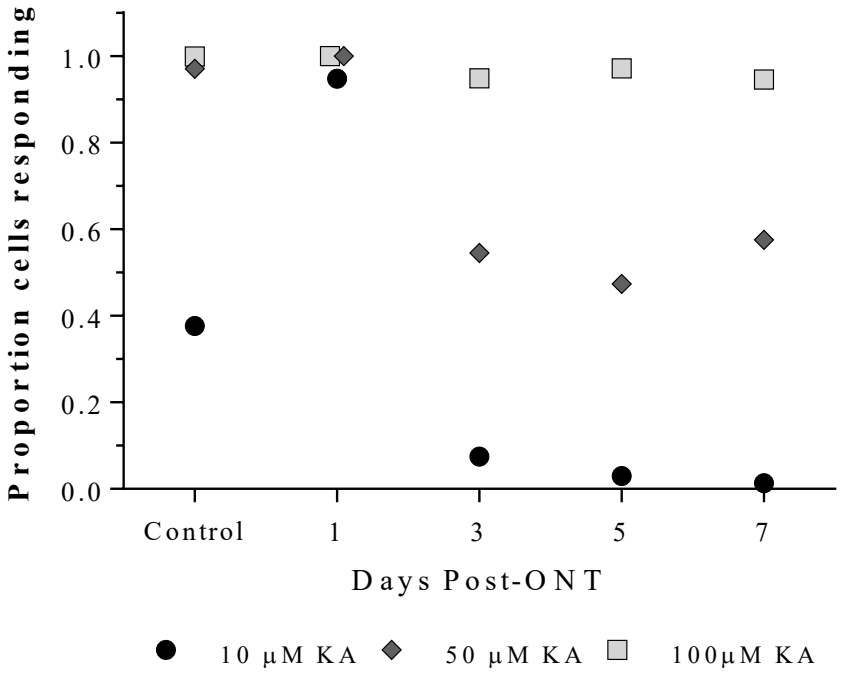

Figure 3.9: Compared to controls, fewer cells responded to extracellular KA with increased time after ONT. Pooled data (from all experiments conducted) show the total proportion of cells that had a change F/F0*100>10 to 10 µM (black circles), 50 µM (dark gray diamonds), and 100 µM (light gray squares) KA. In general, the number of cells responding to KA decreased as length of time post-ONT increased.

time point following ONT and at each KA concentration tested. At 10 μM KA, a relatively small proportion of cells responded in control retinas, whereas nearly all responded 1 day post-ONT. From day 3 to 5 post-ONT the proportion of cells responded continued to decline. At 50 μM KA, virtually all of the cells in control retinas, and in retinas 1 day post-ONT responded. In contrast, the proportion of responders was reduced 3, 5 and 7 days post-ONT. At 100 μM KA, nearly all cells responded at all time points. These data suggest that in the presence of axonal injury, fewer cells are able to respond to lower concentrations of KA following ONT.

Table 3.3 Percent of cells responding to each concentration of KA at each time point

Concentration	**Percent of Total Cells Responding**				
	Control	**Day 1**	**Day 3**	**Day 5**	**Day 7**
10 μM	37.64	94.77	7.47	2.96	1.35
50 μM	97.00	100.00	54.47	47.34	57.54
100 μM	99.90	100.00	94.84	97.14	94.53

3.4 RGC Density in the Presence and Absence of ONT

Another possible advantage to using Thy1-GCaMP3 transgenic animals is that, during longitudinal studies where there is loss of RGCs, GCaMP3^{+} cells could be quantified as a measure of RGC density. To determine if this is the case in our ONT experiments, all GCaMP^{+} cells were counted during each Ca^{2+} imaging experiment to determine whether the density of GCaMP3^{+} cells declined as expected after ONT. GCaMP3^{+} cell densities observed in live tissue imaging experiments decreased with the same trend observed in immunohistochemistry experiments (Figure 3.10). Mean density

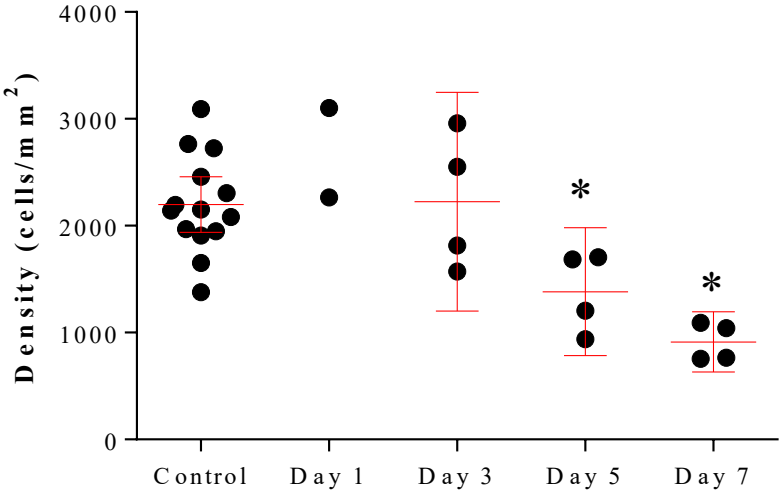

Figure 3.10: Fewer GCaMP3^{+} cells were available for Ca^{2+} imaging. Mean GCaMP3+ cell density did not change compared to control values 1 or 3 days after ONT. Cell density was significantly reduced at both 5 and 7) days post-ONT compared to control (one-way ANOVA; *$p<0.05$). n=74-303 cells/experiment.

(cells/mm^2) observed in retinas 1 (2684) or 3 (2198 ± 261) days post-ONT were not different ($p>0.05$) compared to control (2224 ± 1022), but were significantly different at 5 (1383 ± 598) and 7 (913 ± 283) days post-ONT ($p<0.05$). This indicates that GCaMP3$^+$ RGC decline following ONT was detectable in our live tissue imaging experiments.

Next, to determine whether the decrease in GCaMP3$^+$ cell density observed in live imaging experiments was a good estimate of overall loss of RGCs, and to determine quantitatively whether GCaMP3 expression is specific to RGCs, additional immunohistochemical experiments were conducted. Triple labeling immunohistochemistry, using antibodies against RBPMS to label RGCs and against ChAT to label cholinergic amacrine cells, was performed on control and ONT retinas (Figure 3.11). In the GCL, in both control and ONT retinas, most GCaMP3$^+$ cells were RBPMS-immunoreactive but not ChAT immunoreactive. The mean density of GCaMP3$^+$ cells in control retinas was 2609 ± 481 cells/mm^2 (Figure 3.11A). In these same retinas, the mean density of RBPMS$^+$ RGCs was 3462 ± 557 cells/mm^2 (Figure 3.11A), and 64 ± 4% of RBPMS$^+$ RGCs were also GCaMP3$^+$.

In animals that underwent ONT, there was a downward trend, with time after ONT, in the density of GCaMP3$^+$ cells in ONT eyes, but not in fellow eyes (Figure 3.11A, Table 3.4). This trend was also observed with RBPMS$^+$ cell density following axotomy in ONT eyes (Figure 3.11A). The density of ChAT$^+$ cells did not appear to change after ONT in either ONT eyes or fellow eyes (Figure 3.11A), suggesting that amacrine cells were not sensitive to retinal damage caused by axotomy.

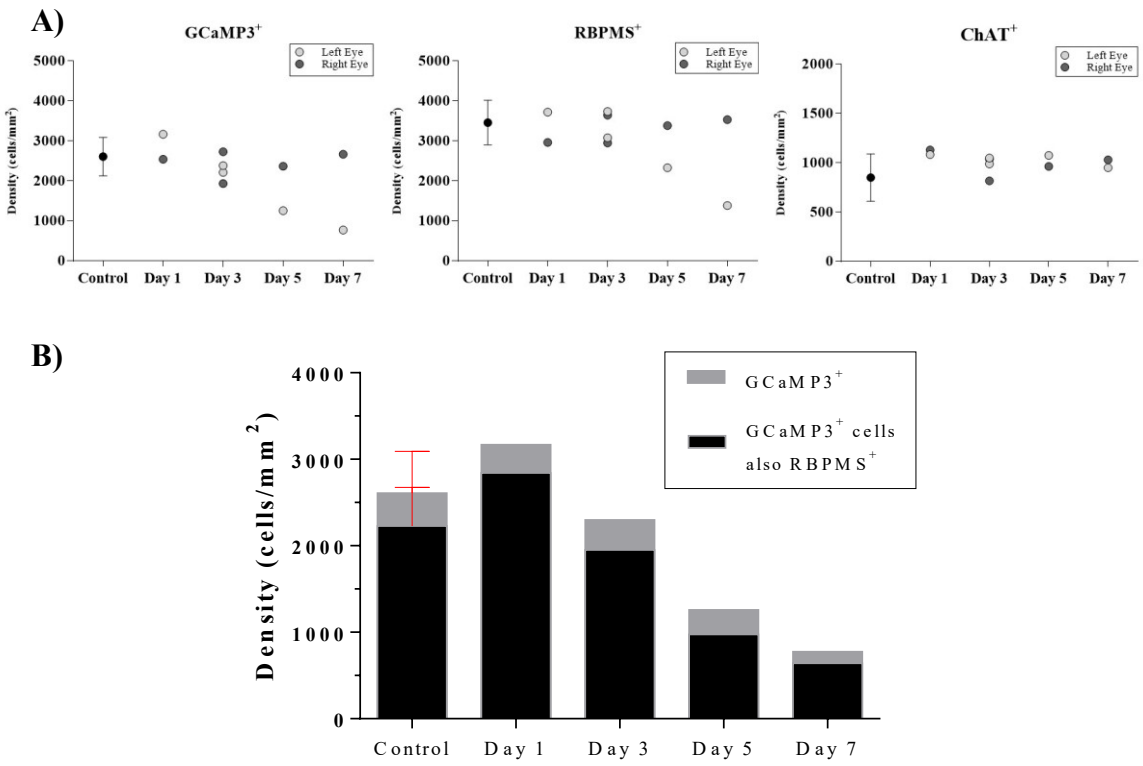

Figure 3.11: GCaMP3 fluorescence was observed in RGCs and not cholinergic amacrine cells. **A)** The density of GCaMP3$^+$ and RBPMS$^+$ in ONT eyes displayed a downward trend with increased length of time following ONT, whereas the density of ChAT$^+$ cells did not. Cell densities in fellow eyes did not appear to change. **B)** Quantification suggests that the proportion of GCaMP3$^+$ cells (gray bars) that were also RBPMS$^+$ (black bars) did not change meaningfully following ONT. Error bars represent upper limit of a 95% CI. Sample sizes (in number of retinas): control = 10; Day 1: 1 ONT, 1 fellow; Day 3: 2 ONT, 2 fellow; Day 5: 1 ONT, 1 fellow; Day 7: 1 ONT, 1 fellow.

Table 3.4 Cell densities (in cells/mm^2) obtained for each label at each time point in ONT and fellow eyes. Data are represented as mean ± ME (margin of error for a 95% confidence interval) where applicable

		Day 1		Day 3		Day 5		Day 7	
Label	**Control**	**ONT**	**Fellow**	**ONT**	**Fellow**	**ONT**	**Fellow**	**ONT**	**Fellow**
GCaMP3	2609±481	3169	2542	2299	2334	1258	2307	774	2667
RBPMS	3462±557	3725	2965	3410	3298	2332	3386	1386	3535
ChAT	850±240	1084	1130	1019	927	1075	964	951	1030

In control retinas, most GCaMP$^+$ cells were RBPMS$^+$ and very few were ChAT$^+$. Of the total population of GCaMP$^+$ cells, 85 ± 6% were RBPMS$^+$ (Figure 3.11B and Table 3.5) and 0.08 ± 0.08% (1.67 ± 2.21 cells/mm^2) were ChAT$^+$. These results suggest that GCaMP3 is expressed in RGCs, and not in cholinergic amacrine cells. In the presence of ONT this appears to also be the case, as the proportion of GCaMP3$^+$ cells that are also RBPMS$^+$ or ChAT$^+$ do not seem to change drastically (Figure 3.11B and Table 3.5). After ONT GCaMP3$^+$ cells were still rarely colocalized with ChAT. These results suggest that the proportion of GCaMP3$^+$ cells that co-express RBPMS or ChAT does not change following ONT.

Table 3.5 Percent of the GCaMP3$^+$ population colocalizing with RBPMS or ChAT. Data are represented as mean ± ME (margin of error for a 95% confidence interval) where applicable

	Control	**Day 1**	**Day 3**	**Day 5**	**Day 7**
Percent GCaMP$^+$ also RBPMS$^+$	85.09 ± 5.70	89.63	84.75	77.42	82.96
Percent GCaMP$^+$ also ChAT$^+$	0.08 ± 0.08	0	0.02	0	0.08

Chapter 4: Discussion

Calcium imaging of retinal ganglion cells in normal and experimental conditions has been a general interest of our laboratory for a long time. Though over the years, the techniques to introduce calcium indicator dyes into RGCs have been refined, selectivity for RGCs still remains an issue. Transgenic mice expressing fluorescent proteins under the Thy1 promoter have been useful in anatomical studies, but until recently, no such animal was available for use in functional calcium imaging experiments. The Thy1-GCaMP3 transgenic mouse has the potential to be extremely useful for future retina research as it allows the possibility of longitudinal anatomical and functional studies in the same animal.

4.1 Overall Expression Pattern of GCaMP3 in Thy1-GCaMP3 Transgenic Mice

Initial data suggested the possibility that GCaMP3 expression is restricted to RGCs (Chen et al., 2012); therefore, an anatomical characterization of its expression in the retinas of these transgenic mice was conducted. These data show that GCaMP3 fluorescence is widely and uniformly distributed throughout the retina of Thy1-GCaMP3 transgenic mice, in neurons located in the GCL, and in a small number of neurons in the INL (Figure 3.1). We also show that GCaMP3 fluorescence is located in the cytoplasm of neuron somas and neurites, and is excluded from the nuclei (Figure 3.1B). These data are in accordance with the limited amount of data published on this transgenic mouse line. Chen and colleagues (2012), the group that developed and conducted the initial characterization of the transgenic line, described that in the retina GCaMP3^{+} neurons were present in the GCL, and were present to a lesser extent in the INL. They also report strong fluorescence observed in the soma and neurites but not the nucleus of cells

expressing GCaMP3 (Chen et al., 2012). These data show that the expression pattern of the founder line is the same as what is now commercially available, and has not changed through several generations of breeding. Therefore, we can be confident that this transgenic mouse line will remain a suitable model for Ca^{2+} imaging for the foreseeable future.

4.2 Functional Performance of GCaMP3

At the functional level, Ca^{2+} transients evoked by the superfusion of 10 μM, 50 μM and 100 μM of kainic acid (KA) were reported by GCaMP3. Fluorescent signals increased following the application of KA and returned to baseline once KA was washed out (Figure 3.2). Transient amplitudes increased in a concentration-dependent manner in response to increasing concentrations of KA. Overall, response amplitudes remained the smallest after application of 10 μM KA, increased with the application of 50 μM KA, and were highest after application of 100 μM KA. This response is also typical of RGCs examined using chemical calcium indicator dyes in control retinas of mice and other mammals (Leinders-Zufall et al., 1994; Baldridge, 1996; Hartwick et al., 2008). Evidence suggests that this increase in Ca^{2+} following non-NMDA receptor stimulation by KA is caused both by the influx from the extracellular space, as well as the efflux from intracellular stores (Leinders-Zufall et al., 1994). The KA concentration-dependent increase is mediated by the increase in molecules available to bind to the receptors at the higher concentrations. The data presented here indicate that GCaMP3 is functional, and that differing amplitudes of calcium transients that result as a consequence of AMKA/kainate receptor stimulation by differing amounts of agonist are reported by GCaMP3 consistently.

4.2.1 Comparison of GCaMP3 with Fura-2

The main objective of this project was to characterize the functional properties of GCaMP3 expressed in the Thy1-GCaMP3 transgenic mouse line in a model of RGC injury, ONT. We first compared the performance of genetically expressed GCaMP3 to a current popular method of Ca^{2+} imaging, namely fura-2 Ca^{2+} indicator dye. Transient amplitudes evoked by the application of 50 μM KA were quantified at one, three, five, and seven days post-ONT.

First, in transgenic animals, robust changes in fluorescence were visible in retinas from control animals, and animals sacrificed one day post-ONT (Figure 3.4). However, after ONT transients reported by GCaMP3 after ONT decreased significantly between one and three days post-ONT, and remained low three to five days post-ONT (Figure 3.4 and 3.5A, Table 3.1). Additionally, three, five and seven days post-ONT transient amplitudes in the uninjured fellow eye were consistently larger than those in the ONT eye, but smaller compared to control retinas (Table 3.1).

The pattern of changes in Ca^{2+} transient amplitude observed in the transgenic genotype was not entirely replicated in control genotypes. While transient amplitudes at three and five days post-ONT were reduced compared to controls, at seven days post-ONT there was no longer a difference (Figure 3.5B, Table 3.1). To my knowledge, there are no published reports investigating changes in calcium transients measured by chemical calcium indicators following ONT, however calcium transients have been shown to be altered in experimental glaucoma models. First in a rat model of experimental glaucoma, two weeks after laser photocoagulation the total area of axons undergoing neurodegeneration was significantly larger compared to control and

correlated with the degree of IOP elevation. In this model, transient amplitudes in RGCs measured by fura-2 in response to the application of ATP (a purinergic receptor agonist) were lower compared to controls, suggesting that damage results in decrease in responsiveness of RGCs (Niittykoski et al., 2010). However, in a separate rat model of glaucoma, with elevated IOP caused by injection of hypertonic saline into an episcleral vein, no difference in responsiveness to NMDA or glutamate was found (Hartwick et al., 2005). The discrepancies between these results and the results obtained in this study may have resulted from different methodologies, including the model of damage induced, as experimental glaucoma is a less severe model of axon damage compared to ONT, as well as techniques to load fura-2 into RGCs.

In GCaMP3 mice, at three, five and seven days post-ONT transient amplitudes in the un-operated fellow eye were also significantly reduced compared to controls (Table 3.1). This was also apparent three days post-ONT in C57Bl/6 mice. This is likely due to inflammation caused by ONT. Retinas from axotomized eyes do display an upregulation of RNA for genes involved in inflammatory pathways suggesting that immune and inflammatory processes play a role in ONT-induced RGC damage (Agudo et al., 2008). It has also been shown that optic nerve injury procedures in one eye can induce an inflammatory response in the contralateral eye (Bodeutsch et al., 1999). This is likely induced by the carriage of inflammatory mediators into the contralateral eye through the bloodstream (Bodeutsch et al., 1999). Therefore, this evidence suggests that ONT produces effects outside the confines of the affected eye. As a result, using contralateral eyes in animals that undergo ONT procedures are not representative as true controls, and should always be accompanied by additional experiments in non-operated control groups.

The differences between transgenic and non-transgenic animals obtained in the current study may have also resulted due to the method used to load fura-2 into GCL neurons. Ca^{2+} transients in C57Bl/6 retinas were imaged using fura-2 introduced to GCL neurons by electroporation. This technique leads to dye loading in RGCs and also amacrine cells (Daniels and Baldridge, 2010; Baden et al., 2016). Therefore, it is possible that transient amplitudes remain higher in control genotypes because of the presence of amacrine cells in the sample population, which are responsive to KA stimulation and unaffected by ONT (Nadal-Nicolás et al., 2015). Previous studies utilizing electroporation to load GCL neurons with calcium indicator dye excluded presumptive amacrine cells on the basis of morphology (smaller size and lack of axon) and stereotyped physiological responses to light stimuli (Daniels and Baldridge, 2010; Baden et al., 2016). In the current study, these methods of exclusion proved difficult. First, physiological characterization based on responses to light stimuli was not possible with the experimental setup employed in this thesis. Second, though overall, amacrine cells tend to be smaller than RGCs, the range of soma diameters of amacrine cells and RGCs do overlap (Jeon et al., 1998). This makes it very difficult to distinguish between large amacrine cells and small RGCs based on morphology (Sun et al., 2002). In ONT groups, the decline in cell density of RGCs only means that the ratio of amacrine cells in the imaging field likely increases with increased time after ONT. This likely accounts for why transient amplitudes at seven days post-ONT do not differ from to controls in C57Bl/6 retinas imaged using fura-2.

4.2.2 Baseline GCaMP3 Fluorescence

An additional source for the discrepancy between transient amplitudes obtained from transgenic and non-transgenic animals is the possibility that the expression level or function of GCaMP3 is altered following ONT. There is evidence to suggest that Thy1-driven gene expression is differentially regulated following optic nerve trauma (Schlamp et al., 2001). For this reason, it was determined whether ONT affected the baseline fluorescence emitted by GCaMP3. If baseline fluorescence was altered following ONT, this would provide evidence suggesting that axonal injury perturbs GCaMP3 expression level or the ability of the protein to reliably report intracellular calcium levels.

Results of the present study show that baseline fluorescence reported by GCaMP3 did not change up to seven days post-ONT (Figure 3.6), suggesting that both the expression level and stability of GCaMP3 persist one week following axonal injury. This result is promising, as fluorescent proteins as well as the expression of some RGC-specific genes do not always remain stable following axonal damage. For example, blood-retinal barrier damage has been shown to quench YFP fluorescence when optic nerve damage is induced (Wang et al., 2011). Additionally, expression of Brn3a, a transcription factor commonly used as a marker of RGCs, is induced in non-RGC cell types following ONT (Nuschke et al., 2015). So far, our data are contrary to this, and suggest that GCaMP3 expression under the Thy1-promoter is stable and does not change drastically following ONT. However, we cannot be entirely sure that this is indeed the case without directly quantifying GCaMP3 protein levels. Interestingly, these results also suggest that resting $[Ca^{2+}]_i$ also remained stable following ONT.

At present, many models of cell death involve cytoplasmic Ca^{2+} overload. For example, in proposed excitotoxicity models, prolonged receptor stimulation leads to over-influx of Ca^{2+} from the extracellular space, and excess extrusion from the ER (Choi, 1994). Additionally, in ROS-triggered cell death, Ca^{2+} extrusion from the ER causes a rise in cytoplasmic $[Ca^{2+}]$ (Graier et al., 1998). In fact, elevated levels of cytoplasmic Ca^{2+} levels are not only known triggers of cell death pathways, but is also a condition that persists during the execution of the pathways (Orrenius et al., 2003; Proskuryakov et al., 2003). Therefore, the results presented here come as a surprise. In retinas that have undergone ONT, a significant proportion of them end up dying as a result of the trauma; by seven days post-injury approximately 50% of RGCs survive, and by 14 days post-ONT only a very small minority survive (Berkelaar et al., 1994). Therefore, at any given time after the procedure, populations of cells that are undergoing the cell death process should be present and included in calcium imaging experiments. Therefore we would expect to see a rise in overall baseline $[Ca^{2+}]_i$ inferred by an increase in GCaMP3 emitted fluorescence. However, we find no evidence of this at any time point post-ONT.

Several factors may account for this, including intracellular Ca^{2+} handling, and methods used to detect changes in basal GCaMP3 fluorescence level. First, excess Ca^{2+} in the cytoplasm is sequestered into mitochondria, where it is capable of initiating and causing the progression cell death programs (Qian et al., 1999; Orrenius et al., 2003; Pan et al., 2014). Furthermore, the mitochondrial Ca^{2+} uniporter displays higher conductance when extramitochondrial Ca^{2+} levels rise (Kirichok et al., 2004). Therefore, it is possible that the excess in cytoplasmic Ca^{2+} caused by axon trauma is sequestered into mitochondria, and this acts as the trigger for cell death in RGCs in cases of ONT.

Additionally, at least one Ca^{2+}-binding protein, calpain, is upregulated in apoptosis (Ray et al., 2000). Therefore, there may also be others. If the Ca^{2+} ions contributing to the overload are being bound by calcium-activated effectors known to contribute to the progression of cell death pathways, like calpain, cell death would still progress and Ca^{2+} levels reported by GCaMP3 may not be noticeably higher due to competition with additional Ca^{2+} binding proteins upregulated during the course of apoptosis and necrosis. Alternatively, if the expression of GCaMP3 is in fact decreased following ONT, cytoplasmic levels of Ca^{2+} may indeed be higher than controls, as together, these factors would present as no net change in non-stimulated GCaMP3 fluorescence. At this point, we are unable to determine for certain whether one, or all, of these factors account for the data observed.

Determining if these factors influenced results obtained in this study is beyond the abilities of the methods employed. The results obtained in the present study suggest that baseline fluorescence level reported by GCaMP3 was not altered by ONT. While these results show promise for measuring Ca^{2+} transients after axonal injury, further studies are required to determine whether GCaMP3 expression changes after ONT and to determine whether Ca^{2+} transient amplitudes are influenced by differing levels of GCaMP3 in the cytoplasm. Nevertheless, our results imply that GCaMP3 remains capable of persistently and accurately monitoring intracellular calcium dynamics in RGCs in both normal and pathological conditions.

4.2.3 Characterization of Ca^{2+} transients reported by GCaMP3 after ONT

Once it was established that GCaMP3 fluorescence did not change following ONT, the amplitude of Ca^{2+} transients evoked by extracellular KA was investigated to

determine whether there were differences between axotomized and control retinas. First, in the present study, one day post-ONT Ca^{2+} transients were variably increased or decreased compared to controls (Figure 3.7, Table 3.2), depending on the concentration of KA applied. This may be representative of an underlying temporal change in RGC responsiveness to extracellular glutamate. Recent evidence indicates that cells undergoing apoptosis in may exhibit altered responsiveness to excitatory amino acid neurotransmitters as a result of increased extracellular levels of said neurotransmitters induced by death of neighbouring cells (Wang et al., 2016b). At acute time points (0-48 hours) following induction of neuronal pathology, expression of the GluR2 subunit increases, suggesting an increase in Ca^{2+} permeability of AMPA receptors (Wang et al., 2016b). This may account for the increase in responses observed with certain concentrations of KA at one day post-ONT. It is also conceivable that at a certain point (between two and three days after injury), there may be a shift in AMPA/Kainate receptor expression or responsiveness as a result of, or in response to progression along the cell death pathway. Alternatively, this shift may be caused by an accumulation of extracellular glutamate left behind by neighbouring dead cells, leading to an overall downregulation of glutamate receptors (Yoles and Schwartz, 1998; Wang et al., 2016b). A shift in responsiveness or expression of receptors would account for the changes observed between one and three days post-ONT (Table 3.2), and the continued reduction in calcium transients up to seven days post-ONT (Figure 3.8 and Table 3.2).

This is not the first piece of evidence suggesting RGC dysfunction precedes cell death. Evidence suggesting functional loss in mouse RGCs following optic nerve trauma has been suggested by studies examining the effect of ONT on the electroretinogram

(ERG) waveform. Specifically, both the negative and positive scotopic threshold response components of the full field mouse ERG have been linked to RGC function (Smith et al., 2014), and decrease in amplitude as early as three days following ONT (Alarcón-Martínez et al., 2010; Smith et al., 2014; Yukita et al., 2015). These results were similar to those obtained in the current study. The changes in Ca^{2+} dynamics in response to extracellular stimulation reported in this thesis are likely indicative of general cellular dysfunction occurring after ONT, and may also contribute to widespread defects in cellular processes mediated by proper Ca^{2+} handling including firing properties, neurotransmitter release onto target structures, and gene expression. At a systemic level, these defects may manifest as reduction in or even loss of visual function occurring prior to the actual death of the cell.

Finally, we observed many cells that were unable to respond to modest concentrations of KA that were still present three to seven days after axonal injury (Figure 3.8, Table 3.2). Using immunohistochemical methods only, all labeled cells are often considered viable without regard for function. Many published works rely solely on immunohistochemical assessment of RGC health and evaluation of putative treatments (Berkelaar et al., 1994; Chidlow et al., 2011; Nadal-Nicolás et al., 2015; Sánchez-Migallón et al., 2016, to name a few). Though these methods give important insights into gross changes in the anatomy of the retina, overall health is likely overestimated by immunohistochemical methods alone. The current research suggests that neuronal dysfunction at a cellular level, manifested as the loss of ability to respond to external stimuli is widespread and precedes the anatomical loss of RGCs detected using immunohistochemical methods in animal models. Therefore, functional measurements of

RGC function should always accompany anatomical data when evaluating the health of RGCs to avoid overestimation of retinal health. Furthermore, these results suggest that complete loss of function precedes anatomical loss.

4.3 RGC Density Decreases after ONT and is Detected in Live Tissue Imaging Experiments

It is well documented that following axonal injury RGC density is reduced. Therefore, to ensure that the decline in RGC density following ONT is mirrored in live imaging experiments, the number GCaMP3-expressing neurons was counted in the field of view from each calcium imaging experiment. These data show that based on these counts, $GCaMP3^+$ cell density was significantly decreased five and seven days post-ONT (Figure 3.9). This result is in accordance with previously published results (Williams et al., 1996; Jeon et al., 1998; Raymond et al., 2008; Wang et al., 2010; Rodriguez et al., 2014), as well as the immunohistochemical results presented in this thesis.

In immunohistochemistry experiments, densities of $GCaMP3^+$ neurons in the GCL of control retinas reported in this study were comparable to previously published densities of CFP expression driven by the Thy1-promoter (Figure 3.10C; Raymond et al., 2008; Wang et al., 2010). Additionally, the density of $RBPMS^+$ RGCs was also comparable to previously published data on RGC densities in C57Bl/6 mice, using both similar and different labeling techniques (Figure 3.10C; Williams et al., 1996; Jeon et al., 1998; Wang et al., 2010; Rodriguez et al., 2014). Consistent with the hypothesis that GCaMP3 is expressed in RGCs, there was a large degree of overlap between $GCaMP^+$ and $RBPMS^+$ cells. However, the density of $GCaMP3^+$ cells was lower than the density of $RBPMS^+$ cells. The data presented show that in control Thy1-GCaMP3 retinas ~64%

of RBPMS$^+$ RGCs were also GCaMP3$^+$, suggesting that only a subset of RGCs express GCaMP3. The proportion of RBPMS$^+$ cells that exhibited GCaMP3 fluorescence reported here is lower than that observed in Thy1-CFP transgenic mouse retinas where ~82% of RBPMS$^+$ cells contained CFP fluorescence (Rodriguez et al., 2014). The difference in expression pattern between the Thy1-GCaMP3 and Thy1-CFP mice compared here can be explained by the fact that the Thy1 promoter does not always drive transgene expression in the same populations of neurons due to transgene position-effects (Feng et al., 2000). Nevertheless, these data indicate that much like in other transgenic models, GCaMP3 is widely expressed throughout the retina at high densities, and represents a major subset of the total GCL neuron population.

In this study, the density of both GCaMP3$^+$ and RBPMS$^+$, but not ChAT$^+$ cells displayed a downward trend with increased time after ONT (Figure 3.10C), consistent with reports indicating that optic nerve injury affects RGCs and not amacrine cells (Nadal-Nicolás et al., 2015). Previous reports indicate that a significant decrease in RGC density is observed after five days post-ONT and by seven days post-ONT approximately 50% of RGCs remain detectable (Berkelaar et al., 1997). Though our sample sizes did not reach high enough numbers for statistical analysis this general trend is observed (Figure 3.10C). Interestingly, in Thy1-CFP mice, Wang et al (2010) observed that CFP$^+$ cells were more resistant to ONT and did not decline at the same rate as Fluoro-gold™ labeled RGCs, indicating that CFP may, at this point, be expressed in other cell types other than RGCS. It is also possible that CFP may be expressed in resilient subtypes of RGCs or fluorescence may persist in cells no longer viable. Our data did not follow this pattern, as GCaMP3$^+$, along with RBPMS$^+$, cell density was markedly reduced by seven days post-

ONT (Figure 3.10C). Again, these differences likely arise from differential expression patterns observed using the Thy1 promoter. These results show that GCaMP3 fluorescence is lost at an expected rate similar to the loss of RGCs measured by RBPMS immunoreactivity, and suggest that GCaMP3 in the Thy1-GCaMP3 transgenic mouse may be expressed in a subset of RGCs representative of the entire population.

Calculated cell densities from Ca^{2+} imaging experiments were somewhat different than densities calculated in immunohistochemistry experiments, as well as densities observed in the Thy1-CFP transgenic mouse for control retinas (Raymond et al., 2008; Wang et al., 2010). This is likely due to the fact that in live imaging experiments only one region was counted, whereas in immunohistochemistry experiments many more regions that accounted for ~10% of the total retina area were counted and averaged together, giving a more precise representation of RGC density. It is possible that regions selected for calcium imaging, in general, were of regions that did not necessarily reflect the average density across the entire retina. Nevertheless, obtaining density measurements from Ca^{2+} imaging experiments still gave an accurate estimate of the degree and progression of cell loss occurring as a result of optic nerve trauma.

Taken together, these observations suggest that under the Thy1 promoter, GCaMP3 is expressed in a large population of GCL neurons, many of which are presumptive RGCs. Furthermore, the population of $GCaMP^{+}$ cells declines similarly to that of $RBPMS^{+}$ cells following ONT, whereas the population of $ChAT^{+}$ amacrine cells remains stable. This evidence further strengthens the hypothesis that GCaMP3 is expressed in RGCs. Additionally, the pattern of cell loss displayed in live imaging experiments is representative of the overall pattern of cell loss observed in

immunohistochemical methods. These data indicate that gross tissue pathology is detectable in live imaging experiments, and predicts the trend of RGC death observed with immunohistochemical techniques.

4.4 Immunohistochemical Characterization of GCaMP3$^+$ Cells in the GCL in the Presence and Absence of Axonal Injury.

The Thy1 promoter was initially believed to be an RGC specific promoter, however it has since been shown that it is additionally capable of driving expression in amacrine cells (Barnstable and Dräger, 1984; Feng et al., 2000; Raymond et al., 2008). Specifically, Raymond and colleagues (2008) determined that CFP is expressed in cholinergic amacrine cells in Thy1-CFP transgenic mice. Therefore, co-labeling experiments were conducted to determine whether GCaMP3 expression is restricted to RGCs or whether it is also present in cholinergic amacrine cells.

Results from these experiments suggest that GCaMP3 is not expressed in cholinergic amacrine cells, however it's expression may not be restricted to RGCs. In control Thy1-GCaMP3 retinas, approximately 85% GCaMP3$^+$ neurons in the GCL were also RBPMS$^+$, indicating that the majority of GCaMP3$^+$ cells were RGCs (Figure 3.10D). Additionally, less than 1% of GCaMP$^+$ cells were ChAT$^+$, indicating that GCaMP3 is not significantly expressed in cholinergic amacrine cells. While these results are promising, there is still a minor population of GCaMP3$^+$/RBPMS$^-$ cells that remain unclassified. One explanation for this could be that GCaMP3 is expressed in a population of amacrine cells that are non-cholinergic. Evidence indicates that ~20% of the displaced amacine cells in the mouse retina express ChAT (Jeon et al., 1998). Other major amacrine cell populations include GABAergic and glycinergic cells, therefore additional immunohistochemistry

experiments using antibodies targeted to these populations may help to characterize this population of GCaMP3^{+} cells. Indeed, Raymond et al. (2008) identified CFP^{+} cells that were determined to be GABAergic on the basis of GAD67 (glutamic acid decarboxylase isoform 67, an enzyme in the synthesis pathway of GABA) and GAT-1 (GABA transporter isoform 1) immunoreactivity. However, they conclude that as the majority of cholinergic amacrine cells are also GABAergic, this represents the cholinergic amacrine cell population, which our ChAT immunohistochemistry experiments have ruled out (Brecha et al., 1988; Kosaka et al., 1988; Raymond et al., 2008). There is no evidence, to my knowledge, that suggest that the Thy1 promoter is active in any other amacrine cell populations. An alternative possibility is that this population of GCaMP^{+}/RBPMS^{-} cells represent RGCs that are not labeled by the anti-RBPMS antibody.

RBPMS immunolabeling is believed to account for the entire population of RGCs in mouse retinas (Rodriguez et al., 2014). However, some evidence indicated that the population of GCaMP3^{+}/RBPMS^{-} cells may not be amacrine cells, and may be RGCs that are RBPMS immunonegative. First, many of these cells have identifiable primary neurites characterized as putative axons. Two examples are illustrated in Figure 4.1, where a putative axon is clearly visible and joins a nearby axon bundle. However, identifying a putative axon was not always possible, as GCaMP3 fluorescence is widespread and dense in the GCL, and neurites are often very difficult to follow; for this reason, these observations were not quantified. Nevertheless, they provide evidence that that a small population of RBPMS^{-} RGCs may exist, and may account for at least a portion of the GCaMP3^{+}/RBPMS^{-} cells observed in this study. Additionally, only a small number of GCaMP^{+} cells were located in the INL, and these cells were characterized as

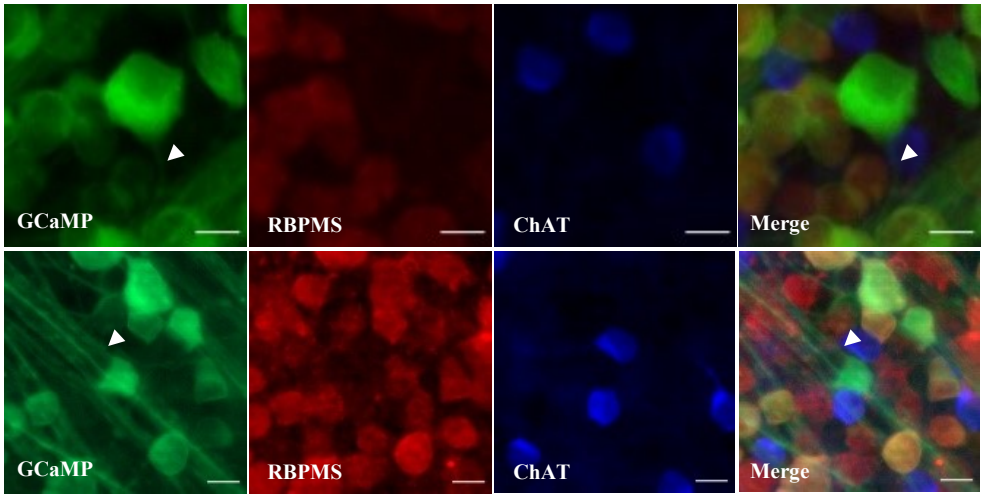

Figure 4.1: Examples of GCaMP^{+}/RBPMS^{-} RGCs. Fluorescence photomicrographs from control retinas of two GCaMP3^{+}/RBPMS^{-} cells where a presumed axon (arrowhead) is visible, indicating that they are RGCs and not amacrine cells. Scale bars = 10 µm.

displaced ganglion cells based on co-labeling with RBPMS (Figure 3.1C). $GCaMP^+/RBPMS^-$ cells in the INL were not observed, suggesting that $GCaMP3^+$ fluorescence may not be in non-cholinergic amacrine cell populations either. However, these observations were not quantified, and do not exclude the likelihood that amacrine cell populations in the GCL differ from those in the INL and therefore express different genes. Further experiments using antibodies targeted to different amacrine cell populations including GABA and glycine are required before the possibility of amacrine cell expression is completely ruled out.

Following ONT, $GCaMP3^+$ fluorescence remained largely co-labeled with RBPMS immunoreactivity (Figure 3.10B and D). At 7 days post-ONT 85% of $GCaMP^+$ neurons were also $RBPMS^+$, and were almost never co-localized with ChAT. These data are very similar to that observed in control retinas. These preliminary quantifications are promising; as discussed previously, optic nerve trauma can cause changes in gene expression and can disrupt fluorophore function. The data presented here suggest that fluorophore function, and GCaMP3 gene expression remained stable following ONT. Additionally, previous studies have shown that CFP fluorescence also is detected in microglia following phagocytosis of dead cells after ONT in the Thy1-CFP mouse (Wang et al., 2010). This would likely interfere with image quality. Fortunately, we did not observe GCaMP fluorescence in non-neuronal cells following ONT, indicating that GCaMP3 fluorescence is eliminated either with cell death or upon phagocytosis.

In summary, these data indicate that most $GCaMP^+$ cells are RGCs and virtually none are cholinergic amacrine cells, and this likely remains the case following ONT. Additionally, GCaMP3 expression appears to remain stable and largely confined to the

RGC population up to seven days post-ONT. Finally, GCaMP3 fluorescence was never observed in glia. Together, these data strengthen the evidence available suggesting that the Thy1-GCaMP3 transgenic mouse line is a valuable research tool for future research in RGC function and dysfunction.

4.5 Future Directions

4.5.1 In Vivo Ca^{2+} Imaging

The data presented here suggest that in the Thy1-GCaMP3 transgenic mouse line, GCaMP3 is able to predictably measure KA-induced Ca^{2+} transients in uninjured RGCs, and is able to report changes in Ca^{2+} transients in retinas subjected to axonal injury using conventional calcium imaging methods. Using a transgenic mouse with a GECI widely expressed in RGCs could provide the unique ability to monitor Ca^{2+} dynamics in populations of cells *in vivo* without the need for invasive and technically challenging procedures to introduce the calcium indicator into the eye such as electroporation and intraorbital injections. In the immediate future, these animals can be imaged *in vivo* using confocal scanning laser ophthalmoscopy, with Ca^{2+} transients stimulated by an ultraviolet LED light stimulus. Additionally, *in vivo* Ca^{2+} imaging can be achieved using two-photon microscopy to image RGC Ca^{2+} dynamics at higher resolution and with easier introduction of an appropriate light stimulus. These imaging techniques, combined with this animal model, provide researchers the unique and novel ability to conduct experiments to investigate the effects of induced RGC dysfunction longitudinally in the same animal to reduce inter-animal variability between time points.

4.5.2 Applicability to Other Animal Models of Retinal Degeneration

GCaMP3 can also be used in other models of retinal degeneration in order to monitor longitudinal changes in Ca^{2+} dynamics in less drastic models of retinal pathology. Though the ONT model is extremely useful in studying RGC pathology, the damage induced is quite severe. Many models of specific retinal pathologies encompass subtler changes in RGC function that occur over more extended periods of time. An excellent example of this is experimental glaucoma induced by an elevation of intraocular pressure. Intraocular pressure can be elevated with relative ease by introducing microbeads into the anterior chamber of the eye to block aqueous outflow (Morgan and Tribble, 2015). This procedure could be done in Thy1-GCaMP3 mice in order to monitor changes in Ca^{2+} dynamics in a model more representative of human pathology than complete ONT.

Furthermore, transgenic animal models of diseases are often used to recapitulate human conditions. If the affected cells are RGCs, these animals could, in theory, be crossed with the Thy1-GCaMP3 transgenic mouse line to generate double transgenic animals with a Ca^{2+} sensitive reporter in RGCs. Additionally, AAV-mediated transfer of genetic material using promoters to specific retinal cell types could be used to introduce GCaMP3 into the retinas of transgenic animal models of ocular disease. Using this technique expression of GCaMP3 can be targeted to cell types other than RGCs, and therefore is applicable to conditions affecting not just RGCs, such as retinitis pigmentosa and Leber's congenital amaurosis, which affect photoreceptors (Morrow et al., 1998). In this regard, the applicability of GCaMP3 as a tool in retinal research is widespread.

4.6 Limitations

The first and most obvious limitation to the work presented in this thesis is the small sample sizes in the ONT immunohistochemistry data. Though the data obtained provide a good basis to begin discussing the anatomical distribution of GCaMP3 following ONT, additional experiments to confirm that the results obtained are not by chance are required before large claims can be made.

A second limitation is the potential contamination of the control genotype fura-2 calcium imaging data with amacrine cell responses. As discussed previously, some amacrine cells are responsive to KA, are not affected by ONT trauma, and are loaded with Ca^{2+} indicator dye by the electroporation protocol used. A way to reduce amacrine cell contamination in the data set would be to impose a minimum size criterion and only include the largest cells in the FOV in the data set. This was considered, however there is an overlap between the size of large amacrine cells, and small RGCs (Jeon et al., 1998). Therefore, by imposing a minimum size criterion, we would be excluding a significant proportion of RGCs, especially in ONT retinas at later time points where there is a significant reduction in RGC density. For this reason, we decided to include all cells within the approximate range of RGC size (~10-25 μm diameter; Sun et al., 2002).

A final limitation of the presented work is that quantification of GCaMP3 protein levels was not done. Therefore, decreases in transient amplitudes reported by GCaMP3 may be a result of decreased protein expression following ONT. However, there was not a decrease in baseline fluorescence reported by GCaMP3 following ONT, which suggests that expression levels remained constant up to seven days post-axotomy. Several factors, such as intracellular Ca^{2+} handling and underlying cytoplasmic Ca^{2+} levels may have

contributed to this result and are discussed above. Nevertheless, based on the methods employed in this thesis expression level appeared to remain stable up to seven days following ONT.

4.7 Conclusion

In degenerative retinal conditions such as glaucoma and diabetic retinopathy, RGCs are affected, and there is the need for a unique way to study them functionally. GCaMP3 is an improvement over calcium indicator dyes because as this research shows, it is likely selectively expressed in RGCs and maintained in the cells and is stable up to seven days after injury. Therefore, future use of this transgenic line as a tool for retina research is promising.

The results presented in this thesis provide interesting insights into the function of RGCs under damaging conditions and suggest that loss of function precedes anatomical loss. This suggests that, evaluating GCL health using only anatomical methods overestimates RGC ability to functionally respond to visual stimuli. Therefore, functional experiments to accompany anatomical data in injury models is critical to developing the most accurate timelines of injury progression. The use of *in vivo* calcium imaging of populations of ganglion cells, which will be made possible by the Thy1-GCaMP3 mouse, will help develop these timelines by allowing functional assessment of RGCs longitudinally with reduced variability between time points.

s

References

Adam Y, Livneh Y, Miyamichi K, Groysman M, Luo L, Mizrahi A (2014) Functional transformations of odor inputs in the mouse olfactory bulb. Front Neural Circuits 8:129.

Agudo M, Pérez-Marín MC, Lönngren U, Sobrado P, Conesa A, Cánovas I, Salinas-Navarro M, Miralles-Imperial J, Hallböök F, Vidal-Sanz M (2008) Time course profiling of the retinal transcriptome after optic nerve transection and optic nerve crush. Mol Vis 14:1050–1063.

Akerboom J, Vélez Rivera JD, Rodríguez Guilbe MM, Alfaro Malave EC, Hernandez HH, Tian L, Hires SA, Marvin JS, Looger LL, Schreiter ER (2009) Crystal Structures of the GCaMP Calcium Sensor Reveal the Mechanism of Fluorescence Signal Change and Aid Rational Design. J Biol Chem 284:6455–6464.

Alarcón-Martínez L, Avilés-Trigueros M, Galindo-Romero C, Valiente-Soriano J, Agudo-Barriuso M, Villa P de la, Villegas-Pérez MP, Vidal-Sanz M (2010) ERG changes in albino and pigmented mice after optic nerve transection. Vision Res 50:2176–2187.

Antonetti DA, Klein R, Gardner TW (2012) Diabetic Retinopathy. N Engl J Med 366:1227–1239.

Babcock DF, Herrington J, Goodwin PC, Park YB, Hille B (1997) Mitochondrial participation in the intracellular calcium network. J Cell Biol 136:833–844.

Baden T, Berens P, Franke K, Roman-Roson M, Bethge M, Euler (2016) The functional diversity of mouse retinal ganglion cells. Nature 529:1–21.

Baird GS, Zacharias DA, Tsien RY (1999) Circular Permutation and Receptor Insertion within Green Fluorescent Protein. Proc Natl Acad Sci U S A 96:11241–11246.

Baldridge WH (1996) Optical Recordings of the Effects of Cholinergic Ligands on Neurons in the Ganglion Cell Layer of Mammalian Retina. J Neurosci 16:5060–5072.

Bansal A, Singer JH, Hwang BJ, Xu W, Beaudet A, Feller MB (2000) Mice lacking specific nicotinic acetylcholine receptor subunits exhibit dramatically altered spontaneous activity patterns and reveal a limited role for retinal waves in forming ON and OFF circuits in the inner retina. J Neurosci 20:7672–7681.

Barber AJ, Lieth E, Khin SA, Antonetti DA, Buchanan AG, Gardner TW (1998) Neural apoptosis in the retina during experimental and human diabetes: Early onset and effect of insulin. J Clin Invest 102:783–791.

Barnstable CJ, Dräger UC (1984) Thy-1 antigen: A ganglion cell specific marker in rodent retina. Neuroscience 11:847–885.

Berkelaar M, Clarke DB, Wang Y-C, Bray GM, Aguayo AJ (1994) Axotomy Ganglion Results in Delayed Death and Apoptosis of Retinal Cells in Adult Rats. J Neurosci 14:4368–4374.

Bloomfield SA, Dowling JE (1985) Roles of aspartate and glutamate in synaptic transmission in rabbit retina. I. Outer plexiform layer. J Neurophysiol 53:699–713.

Bodeutsch N, Siebert H, Dermon C, Thanos S (1999) Unilateral injury to the adult rat optic nerve causes multiple cellular responses in the contralateral site. J Neurobiol 38:116–128.

Bommert K, Charlton MP, DeBello WM, Chin GJ, Betz H, Augustine GJ (1993) Inhibition of Neurotransmitter Release by C2-domain Peptides Implicates Synaptotagmin in Exocytosis. Nature 363:163–165.

Brecha N, Johnson D, Peichl L, Wassle H (1988) Cholinergic amacrine cells of the rabbit retina contain glutamate decarboxylase and gamma-aminobutyrate immunoreactivity. Proc Natl Acad Sci U S A 85:6187–6191.

Briggman KL, Euler T (2011) Bulk electroporation and population calcium imaging in the adult mammalian retina. J Neurophysiol 105:2601–2609.

Brini M, Calì T, Ottolini D, Carafoli E (2014) Neuronal calcium signaling: Function and dysfunction. Cell Mol Life Sci 71:2787–2814.

Brini M, Carafoli E (2011) The plasma membrane Ca2+-ATPase and the plasma membrane sodium calcium exchanger cooperate in the regulation of cell calcium. Cold Spring Harb Perspect Biol 3.

Chen Q, Cichon J, Wang W, Qiu L, Lee SR, Campbell NR, Destefino N, Goard MJ, Fu Z, Yasuda R, Looger LL, Arenkiel BR, Gan W-B, Feng G (2012) Imaging Neural Activity Using Thy1-GCaMP Transgenic Mice. Neuron 76:297–308.

Chen T-W, Wardill TJ, Sun Y, Pulver SR, Renninger SL, Baohan A, Schreiter ER, Kerr R a, Orger MB, Jayaraman V, Looger LL, Svoboda K, Kim DS (2013a) Ultrasensitive fluorescent proteins for imaging neuronal activity. Nature 499:295–300.

Chen Y, Song X, Ye S, Miao L, Zhu Y, Zhang R, Ji G (2013b) Structural insight into enhanced calcium indicator GCaMP3 and GCaMPJ to promote further improvement. Protein Cell 4:299–309.

Chidlow G, Ebneter A, Wood JPM, Casson RJ (2011) The optic nerve head is the site of axonal transport disruption, axonal cytoskeleton damage and putative axonal regeneration failure in a rat model of glaucoma. Acta Neuropathol 121:737–751.

Choi DW (1994) Calcium and excitotoxic neuronal injury. Ann N Y Acad Sci 747:162–171.

Cueva Vargas JL, Osswald IK, Unsain N, Aurousseau MR, Barker PA, Bowie D, Di Polo A (2015) Soluble Tumor Necrosis Factor Alpha Promotes Retinal Ganglion Cell Death in Glaucoma via Calcium-Permeable AMPA Receptor Activation. J Neurosci 35:12088–12102.

Dacey D, Packer OS, Diller L, Brainard D, Peterson B, Lee B (2000) Center surround receptive field structure of cone bipolar cells in primate retina. Vision Res 40:1801–1811.

Daniels BA, Baldridge WH (2010) D-Serine enhancement of NMDA receptor-mediated calcium increases in rat retinal ganglion cells. J Neurochem 112:1180–1189.

Deisseroth K, Heist EK, Tsien RW (1998) Translocation of calmodulin to the nucleus supports CREB phosphorylation in hippocampal neurons. Nature 392:198–202.

Dezawa M, Takano M, Negishi H, Mo X, Oshitari T, Sawada H (2002) Gene transfer into retinal ganglion cells by in vivo electroporation: a new approach. Micron 33:1–6.

Díez-García J, Matsushita S, Mutoh H, Nakai J, Ohkura M, Yokoyama J, Dimitrov D, Knöpfel T (2005) Activation of cerebellar parallel fibers monitored in transgenic mice expressing a fluorescent Ca2+ indicator protein. Eur J Neurosci 22:627–635.

Ding JJ, Luo AF, Hu LY, Wang DC, Shao F (2014) Structural basis of the ultrasensitive calcium indicator GCaMP6. Sci China Life Sci 57:269–274.

Dolmetsch RE, Pajvani U, Fife K, Spotts JM, Greenberg ME (2001) Signaling to the nucleus by an L-type calcium channel-calmodulin complex through the MAP kinase pathway. Science 294:333–339.

Dowling JE (2012) The Retina: An Approachable Part of the Brain, Revised. Cambridge, Massachusetts and London, England: The Belknap Press of Harvard University Press.

Edgerton JR, Reinhart PH (2003) Distinct contributions of small and large conductance Ca2+-activated K+ channels to rat Purkinje neuron function. J Physiol 548:53–69.

Faber ESL, Sah P (2002) Physiological role of calcium-activated potassium currents in the rat lateral amygdala. J Neurosci 22:1618–1628.

Feng G, Mellor RH, Bernstein M, Keller-Peck C, Nguyen QT, Wallace M, Nerbonne JM, Lichtman JW, Sanes JR (2000) Imaging Neuronal Subsets in Transgenic Mice Expressing Multiple Spectral Variants of GFP. Neuron 28:41–51.

Fesenko EE, Kolesnikov SS, Lyubarsky AL (1985) Induction by cyclic GMP of cationic conductance in plasma membrane of retinal rod outer segment. Nature 313:310–313.

Foster PJ, Buhrmann R, Quigley HA, Johnson GJ (2002) The definition and classification of glaucoma in prevalence surveys. Br J Ophthalmol 86:238–243.

Gao YR, Greene SE, Drew PJ (2015) Mechanical restriction of intracortical vessel dilation by brain tissue sculpts the hemodynamic response. Neuroimage 115:162–176 Available at: http://dx.doi.org/10.1016/j.neuroimage.2015.04.054.

Gee KR, Brown KA, Chen W-NU, Bishop-Stewart J, Gray D, Johnson I (2000) Chemical and physiological characterization of fluo-4 Ca2+-indicator dyes. Cell Calcium 27:97–106.

Goldberg JA, Wilson CJ (2005) Control of Spontaneous Firing Patterns by the Selective Coupling of Calcium Currents to Calcium-Activated Potassium Currents in Striatal Cholinergic Interneurons. J Neurosci 25:10230–10238.

Graier WF, Hoebel BG, Paltauf-Doburzynska J, Kostner GM (1998) Effects of superoxide anions on endothelial Ca2+ signaling pathways. Arter Thromb Vasc Biol 18:1470–1479.

Grynkiewicz G, Moenie M, Tsien RY (1985) A New Generation Ca2+ Indicators with Greatly Improved Fluorescence Properties. J Biol Chem 260:3440–3450.

Hagins WA, Penn RD, Yoshikami S (1970) Dark current and photocurrent in retinal rods. Biophys J 10:380–412.

Hardingham GE, Arnold FJ, Bading H (2001) Nuclear calcium signaling controls CREB-mediated gene expression triggered by synaptic activity. Nat Neurosci 4:261–267.

Hartwick ATE, Hamilton CM, Baldridge WH (2008) Glutamatergic calcium dynamics and deregulation of rat retinal ganglion cells. J Physiol 586:3425–3446.

Hartwick ATE, Lalonde MR, Barnes S, Baldridge WH (2004) Adenosine A1-receptor modulation of glutamate-induced calcium influx in rat retinal ganglion cells. Invest Ophthalmol Vis Sci 45:3740–3748.

Hartwick ATE, Zhang X, Chauhan BC, Baldridge WH (2005) Functional assessment of glutamate clearance mechanisms in a chronic rat glaucoma model using retinal ganglion cell calcium imaging. J Neurochem 94:794–807.

Holcombe DJ, Lengefeld N, Gole GA, Barnett NL (2008) The effects of acute intraocular pressure elevation on rat retinal glutamate transport. Acta Ophthalmol 86:408–414.

Horikawa K, Yamada Y, Matsuda T, Kobayashi K, Hashimoto M, Matsu-ura T, Miyawaki A, Michikawa T, Mikoshiba K, Nagai T (2010) Spontaneous network activity visualized by ultrasensitive Ca(2+) indicators, yellow Cameleon-Nano. Nat Methods 7:729–732.

Hu SC, Chrivia J, Ghosh A (1999) Regulation of CBP-mediated transcription by neuronal calcium signaling. Neuron 22:799–808.

Hu Y, Park KK, Yang L, Wei X, Yang Q, Cho K-S, Thielen P, Lee A-H, Cartoni R, Glimcher LH, Chen DF, He Z (2012) Differential effects of unfolded protein response pathways on axon injury-induced death of retinal ganglion cells. Neuron 73:445–452.

Jeon CJ, Strettoi E, Masland RH (1998) The major cell populations of the mouse retina. J Neurosci 18:8936–8946.

Kanamori A, Catrinescu M-M, Kanamori N, Mears KA, Beaubien R, Levin LA (2010) Superoxide is an associated signal for apoptosis in axonal injury. Brain 133:2612–2625.

Kaneko A (1970) Physiological and morphological identification of horizontal, bipolar and amacrine cells in goldfish retina. J Physiol 207:623–633.

Kerr JF., Wyllie AH, Currie AR (1972) Apoptosis: A basic biological phenomenon with wide-ranging implications in human disease. Br J Cancer 26:239–257.

Kikuchi M, Tenneti L, Lipton SA (2000) Role of p38 mitogen-activated protein kinase in axotomy-induced apoptosis of rat retinal ganglion cells. J Neurosci 20:5037–5044.

Kirichok Y, Krapivinsky G, Clapham DE (2004) The mitochondrial calcium uniporter is a highly selective ion channel. Nature 427:360–364 Available at: http://www.ncbi.nlm.nih.gov/pubmed/14737170.

Kosaka T, Tauchi M, Dahl JL (1988) Cholinergic neurons containing GABA-like and/or glutamic acid decarboxylase-like immunoreactivities in various brain regions of the rat. Exp Brain Res 70:605–617.

Lam DMK, Lasater EM, Naka K (1978) γ-Aminobutyric acid: A neurotransmitter candidate for cone horizontal cells of the catfish retina. Proc Natl Acad Sci U S A 75:6310–6313.

Leinders-Zufall T, Rand MN, Waxman SG, Kocsis JD (1994) Differential role of two Ca(2+)-permeable non-NMDA glutamate channels in rat retinal ganglion cells: kainate-induced cytoplasmic and nuclear Ca2+ signals. J Neurophysiol 72:2503–2516.

Leonard JP, Salpeter MM (1979) Agonist-induced myopathy at the neuromuscular junction is mediated by calcium. J Cell Biol 82:811–819.

Lev-Tov A, Rahamimoff R (1980) A Study of Tetanic and Post-Tetanic Potentiation of Miniature End-Plate Potentials at the Frog Neuromuscular Junction. J Physiol 309:247–273.

Li Q, Puro DG (2002) Diabetes-Induced Dysfunction of the Glutamate Transporter in Retinal Muller Cells. Invest Ophthalmol Vis Sci 43.

Lieven CJ, Hoegger MJ, Schlieve CR, Levin LA (2006) Retinal ganglion cell axotomy induces an increase in intracellular superoxide anion. Investig Ophthalmol Vis Sci 47:1477–1485.

Littleton JT, Bellen HJ (1995) Synaptotagmin controls and modulates synaptic-vesicle fusion in a Ca(2+)-dependent manner. Trends Neurosci 18:177–183.

MacNeil MA, Heussy JK, Dacheux RF, Raviola E, Masland RH (2004) The population of bipolar cells in the rabbit retina. J Comp Neurol 472:73–86.

MacNeil MA, Masland RH (1998) Extreme diversity among amacrine cells: Implications for function. Neuron 20:971–982.

Markram H, Helm PJ, Sakmann B (1995) Dendritic calcium transients evoked by single back-propagating action potentials in rat neocortical pyramidal neurons. J Physiol 485.1:1–20.

Masland RH (2012) The Neuronal Organization of the Retina. Neuron 76:266–280 Available at: http://dx.doi.org/10.1016/j.neuron.2012.10.002.

Matsuda T, Cepko CL (2004) Electroporation and RNA interference in the rodent retina in vivo and in vitro. Proc Natl Acad Sci U S A 101:16–22.

Minta A, Kao JPY, Tsien RY (1989) Fluorescent indicators for cytosolic calcium based on rhodamine and fluorescein chromophores. J Biol Chem 264:8171–8178.

Miyawaki A, Llopis J, Heim R, McCaffery JM, Adams JA, Ikura M, Tsien RY (1997) Fluorescent indicators for Ca2+ based on green fluorescent proteins and calmodulin. Nature 388:882–887.

Morgan JE, Tribble JR (2015) Microbead models in glaucoma. Exp Eye Res 141:9–14.

Morrow EM, Furukawa T, Cepko CL (1998) Vertebrate photoreceptor cell development and disease. Trends Cell Biol 8:353–358.

Müller B, Peichl L (1993) Horizontal cells in the cone-dominated tree shrew retina: morphology, photoreceptor contacts, and topographical distribution. J Neurosci Off J Soc Neurosci 13:3628–3646.

Munemasa Y, Ahn JH, Kwong JMK, Caprioli J, Piri N (2009) Redox proteins thioredoxin 1 and thioredoxin 2 support retinal ganglion cell survival in experimental glaucoma. Gene Ther 16:17–25.

Muto A, Ohkura M, Abe G, Nakai J, Kawakami K (2013) Real-time visualization of neuronal activity during perception. Curr Biol 23:307–311.

Nadal-Nicolás FM, Sobrado-Calvo P, Jiménez-López M, Vidal-Sanz M, Agudo-Barriuso M (2015) Long-Term Effect of Optic Nerve Axotomy on the Retinal Ganglion Cell Layer. Invest Ophthalmol Vis Sci 56:6095–6112.

Nakai J, Ohkura M, Imoto K (2001) A high signal-to-noise Ca(2+) probe composed of a single green fluorescent protein. Nat Biotechnol 19:137–141.

Nawy S (1999) The metabotropic receptor mGluR6 may signal through Go, but not phosphodiesterase, in retinal bipolar cells. J Neurosci 19:2938–2944.

Ng Y, Zeng X, Ling E (2004) Expression of glutamate receptors and calcium-binding proteins in the retina of streptozotocin-induced diabetic rats. Brain Res 1018:66–72.

Nickerson JM, Goodman P, Chrenek MA, Bernal CJ, Berglin L, Redmond TM, Boatright JH (2012) Subretinal Delivery and Electroporation in Pigmented and Nonpigmented Adult Mouse Eyes. In: Retinal Development: Methods and Protocols in Molecular Biology (Wang S-Z, ed), pp 53–69. Springer Science+Business Media.

Niittykoski M, Kalesnykas G, Larsson KP, Kaarniranta K, Åkerman KEO, Uusitalo H (2010) Altered calcium signaling in an experimental model of glaucoma. Investig Ophthalmol Vis Sci 51:6387–6393.

Nuschke AC, Farrell SR, Levesque JM, Chauhan BC (2015) Assessment of retinal ganglion cell damage in glaucomatous optic neuropathy: Axon transport, injury and soma loss. Exp Eye Res 141:111–124.

Orrenius S, Zhivotovsky B, Nicotera P (2003) Regulation of cell death: the calcium–apoptosis link. Nat Rev Mol Cell Biol 4:552–565.

Palczewski K, Kumasaka T, Hori T, Behnke CA, Motoshima H, Fox BA, Le Trong I, Teller DC, Okada T, Stenkamp RE, Yamamoto M, Miyano M (2000) Crystal Structure of Rhodopsin: A G Protein-Coupled Receptor. Science 289:739–745.

Pan X, Liu J, Nguyen T, Liu C, Sun J, Teng Y, Maria M, Rovira II, Allen M, Springer DA, Aponte AM, Balaban RS, Murphy E, Finkel T (2014) The physiological role of mitochondrial calcium revealed by mice lacking the mitochondrial calcium uniporter (MCU). Nat Cell Biol 15:1–17.

Paredes RM, Etzler JC, Watts LT, Zheng W, Lechleiter JD (2008) Chemical calcium indicators. Methods 46:143–151.

Pascolini D, Mariotti S (2012) Global estimates of visual impairment: 2010. Br J Ophthalmol 96: 614-618.

Paus S, Brecht HM, Köster J, Seeger G, Klockgether T, Wüllner U (2003) Sleep attacks, daytime sleepiness, and dopamine agonists in Parkinson's disease. Mov Disord 18:659–667.

Peichl L, González-Soriano J (1994) Morphological types of horizontal cell in rodent retinae: A comparison of rat, mouse, gerbil, and guinea pig. Vis Neurosci 11:501–517.

Proskuryakov SY, Konoplyannikov AG, Gabai VL (2003) Necrosis: A specific form of programmed cell death? Exp Cell Res 283:1–16.

Qian T, Herman B, Lemasters JJ (1999) The mitochondrial permeability transition mediates both necrotic and apoptotic death of hepatocytes exposed to Br-A23187. Toxicol Appl Pharmacol 154:117–125.

Quigley HA, Davis EB, Anderson DR (1977) Descending optic nerve degeneration in primates. Invest Ophthalmol Vis Sci 16:841–849.

Ray SK, Fidan M, Nowak MW, Wilford GG, Hogan EL, Banik NL (2000) Oxidative stress and Ca2+ influx upregulate calpain and induce apoptosis in PC12 cells. Brain Res 852:326–334.

Raymond ID, Vila A, Huynh U-CN, Brecha NC (2008) Cyan fluorescent protein expression in ganglion and amacrine cells in a thy1-CFP transgenic mouse retina. Mol Vis 14:1559–1574.

Rodriguez AR, Pérez De Sevilla Müller L, Brecha NC (2014) The RNA Binding Protein RBPMS is a Selective Marker of Ganglion Cells in the Mammalian Retina. J Comp Neurol 522:1411–1443.

Russelakis-Carneiro M, Silveira LCL, Perry VH (1996) Factors affecting the survival of cat retinal ganglion cells after optic nerve injury. J Neurocytol 25:393–402.

Sánchez-Migallón MC, Valiente-Soriano FJ, Nadal-Nicolás FM, Vidal-Sanz M, Agudo-Barriuso M (2016) Apoptotic retinal ganglion cell death after optic nerve transection or crush in mice: Delayed RGC loss with BDNF or a caspase 3 inhibitor. Investig Ophthalmol Vis Sci 57:81–93.

Sanes JR, Zipursky SL (2010) Design Principles of Insect and Vertebrate Visual Systems. Neuron 66:15–36.

Santiago AR, Gaspar JM, Baptista FI, Cristóvão AJ, Santos PF, Kamphuis W, Ambrósio AF (2009) Diabetes changes the levels of ionotropic glutamate receptors in the rat retina. Mol Vis15:1620–1630.

Sargoy A, Barnes S, Brecha NC, Pérez De Sevilla Müller L (2014) Immunohistochemical and Calcium Imaging Methods in Wholemount Rat Retina. J Vis Exp:e51396.

Sasaki T, Kaneko A (2007) Elevation of intracellular Ca2+ concentration induced by hypoxia in retinal ganglion cells. Jpn J Ophthalmol 51:175–180.

Schanne FAX, Kane AB, Young EE, Farber JL (1979) Calcium Dependence of Toxic Cell Death : A Final Common Pathway. Am Assoc Adv Sci 206:700–702.

Schlamp CL, Johnson EC, Li Y, Morrison JC, Nickells RW (2001) Changes in Thy1 gene expression associated with damaged retinal ganglion cells. Mol Vis 7:192–201.

Schön C, Biel M, Michalakis S (2015) Retinal gene delivery by adeno-associated virus (AAV) vectors: Strategies and applications. Eur J Pharm Biopharm 95:343–352.

Shao LR, Halvorsrud R, Borg-Graham L, Storm JF (1999) The role of BK-type Ca2+-dependent K+ channels in spike broadening during repetitive firing in rat hippocampal pyramidal cells. J Physiol 521 Pt 1:135–146.

Shen S, Wiemelt AP, McMorris FA, Barres BA (1999) Retinal ganglion cells lose trophic responsiveness after axotomy. Neuron 23:285–295.

Shen Y, Heimel JA, Kamermans M, Peachey NS, Gregg RG, Nawy S (2009) A transient receptor potential-like channel mediates synaptic transmission in rod bipolar cells. J Neurosci 29:6088–6093.

Shiells RA, Falk G, Naghshineh S (1981) Action of Glutamate and Asparate Analogues on Rod Horizontal and Bipolar cells. Nature 294:1689–1699.

Slaughter MM, Miller RF (1983) The role of excitatory amino acid transmitters in the mudpuppy retina: An analysis with kainic acid and N-methyl aspartate. J Neurosci 3:1701–1711.

Smith BJ, Wang X, Chauhan BC, C??t?? PD, Tremblay F (2014) Contribution of retinal ganglion cells to the mouse electroretinogram. Doc Ophthalmol 128:155–168.

Stevens GA, White RA, Flaxman SR, Price H, Jonas JB, Keeffe J, Leasher J, Naidoo K, Pesudovs K, Resnikoff S, Taylor H, Bourne RRA (2013) Global prevalence of vision impairment and blindness: Magnitude and temporal trends, 1990-2010. Ophthalmology 120:2377–2384.

Stryer L (1986) Cyclic Gmp Cascade of Vision. Annu Rev Neurosci 9:87–119.

Sun W, Li N, He S (2002) Large-scale morphological survey of mouse retinal ganglion cells. J Comp Neurol 451:115–126.

Tang P, Zhang Y, Chen C, Ji X, Ju F, Liu X, Gan W-B, He Z, Zhang S, Li W, Zhang L (2015) In vivo two-photon imaging of axonal dieback, blood flow, and calcium influx with methylprednisolone therapy after spinal cord injury. Sci Rep 5:9691.

Tezel G, Yang X, Cai J (2005) Proteomic identification of oxidatively modified retinal proteins in a chronic pressure-induced rat model of glaucoma. Investig Ophthalmol Vis Sci 46:3177–3187.

Tian L, Hires SA, Mao T, Huber D, Chiappe ME, Chalasani SH, Petreanu L, Akerboom J, McKinney S a, Schreiter ER, Bargmann CI, Jayaraman V, Svoboda K, Looger LL (2009) Imaging neural activity in worms, flies and mice with improved GCaMP calcium indicators. Nat Methods 6:875–881.

Tsien RY (1980) New Calcium Indicators and Buffers with High Selectivity against Magnesium and Protons: Design, Synthesis, and Properties of Prototype Structures. Biochemistry 19:2396–2404.

Tsien RY, Pozzan T, Rink TJ (1982) Calcium Homeostasis in Intact Lymphocytes : Cytoplasmic Free Calcium Monitored With a New , Intracellularly Trapped Fluorescent Indicator. J Cell Biol 94:325–334.

Vazquez AL, Murphy MC, Kim S-G (2014) Neuronal and physiological correlation to hemodynamic resting-state fluctuations in health and disease. Brain Connect 4:727–740.

Wang J, Hamm RJ, Povlishock JT (2011) Traumatic axonal injury in the optic nerve: evidence for axonal swelling, disconnection, dieback, and reorganization. J Neurotrauma 28:1185–1198.

Wang X, Archibald ML, Stevens K, Baldridge WH, Chauhan BC (2010) Cyan fluorescent protein (CFP) expressing cells in the retina of Thy1-CFP transgenic mice before and after optic nerve injury. Neurosci Lett 468:110–114.

Wang X, Pinter MJ, Rich MM (2016a) Reversible Recruitment of a Homeostatic Reserve Pool of Synaptic Vesicles Underlies Rapid Homeostatic Plasticity of Quantal Content. J Neurosci 36:828–836.

Wang Y-X, Zhang F, Ma X-L, He C-C, Tian K, Wang H-G, An D, Heng B, Xie L-H, Liu Y-Q (2016b) Oxygen–glucose deprivation enhancement of cell death/apoptosis in PC12 cells and hippocampal neurons correlates with changes in neuronal excitatory amino acid neurotransmitter signaling and potassium currents. Neuroreport 27:617–626.

Wässle H (2004) Parallel processing in the mammalian retina. Nat Rev Neurosci 5:747–757.

Wässle H, Puller C, Müller F, Haverkamp S (2009) Cone contacts, mosaics, and territories of bipolar cells in the mouse retina. J Neurosci 29:106–117.

Weitzman MD, Linden RM (2011) Adeno-Associated Virus Biology. In: Adeno-Associated Virus: Methods and Protocols (Snyder RO, Moullier P, eds), pp 1–23. Springer Science+B.

Werblin FS, Dowling JE (1969) Organization of the retina of the mudpuppy, Neturus maculosis. II. Intracellular recording. J Neurophysiol 32:339–355.

Williams RW, Strom RC, Rice DS, Goldowitz D (1996) Genetic and environmental control of variation in retinal ganglion cell number in mice. J Neurosci 16:7193–7205.

Wong RO, Chernjavsky A, Smith SJ, Shatz CJ (1995) Early functional neural networks in the developing retina. Nature 374:716–718.

Yoles E, Schwartz M (1998) Elevation of intraocular glutamate levels in rats with partial lesion of the optic nerve. Arch Ophthalmol 116:906–910.

Yu J, Daniels BA, Baldridge WH (2009) Slow Excitation of Cultured Rat Retinal Ganglion Cells by Activating Group I Metabotropic Glutamate Receptors. J Neurophysiol 102:3728–3739.

Yukita M, Machida S, Nishiguchi KM, Tsuda S, Yokoyama Y, Yasuda M, Maruyama K, Nakazawa T (2015) Molecular, anatomical and functional changes in the retinal ganglion cells after optic nerve crush in mice. Doc Ophthalmol 130:149–156.

Zhang L, Ino-ue M, Dong K, Yamamoto M (2000) Retrograde axonal transport impairment of large- and medium-sized retinal ganglion cells in diabetic rat. Curr Eye Res 20:131–136.

Zhao Y, Araki S, Wu J, Teramoto T, Chang Y-F, Nakano M, Abdelfattah AS, Fujiwara M, Ishihara T, Nagai T, Campbell RE (2011) An Expanded Palette of Genetically Encoded Ca^{2+} Indicators. Science 333:1888-1891.

Zimmerberg J, Akimov SA, Frolov V (2006) Synaptotagmin: fusogenic role for calcium sensor? Nat Struct Mol Biol 13:301–303.